J. metamorphic Geol., 2002, **20,** 217–237

High-*T*, low-*P* metamorphism in the Palaeoproterozoic Halls Creek Orogen, northern Australia: the middle crustal response to a mantle-related transient thermal pulse

S. BODORKOS,[1,2] M. SANDIFORD,[2] N. H. S. OLIVER[3] AND P. A. CAWOOD[1]
[1]*Tectonics Special Research Centre, Department of Applied Geology, Curtin University of Technology, Perth WA 6845, Australia*
[2]*School of Earth Sciences, University of Melbourne, Melbourne VIC 3010, Australia (bodorkos@unimelb.edu.au)*
[3]*Economic Geology Research Unit, School of Earth Sciences, James Cook University, Townsville QLD 4811, Australia*

ABSTRACT High-*T*, low-*P* metamorphic rocks of the Palaeoproterozoic central Halls Creek Orogen in northern Australia are characterised by low radiogenic heat production, high upper crustal thermal gradients (locally exceeding 40 °C km^{-1}) sustained for over 30 Myr, and a large number of layered mafic-ultramafic intrusions with mantle-related geochemical signatures. In order to account for this combination of geological and thermal characteristics, we model the middle crustal response to a transient mantle-related heat pulse resulting from a temporary reduction in the thickness of the mantle lithosphere. This mechanism has the potential to raise mid-crustal temperatures by 150–400 °C within 10–20 Myr following initiation of the mantle temperature anomaly, via conductive dissipation through the crust. The magnitude and timing of maximum temperatures attained depend strongly on the proximity, duration and lateral extent of the thermal anomaly in the mantle lithosphere, and decrease sharply in response to anomalies that are seated deeper than 50–60 km, maintained for <5 Myr in duration and/or have half-widths <100 km. Maximum temperatures are also intimately linked to the thermal properties of the model crust, primarily due to their influence on the steady-state (background) thermal gradient. The amplitudes of temperature increases in the crust are principally a function of depth, and are broadly independent of crustal thermal parameters.

Mid-crustal felsic and mafic plutonism is a predictable consequence of perturbed thermal regimes in the mantle and the lowermost crust, and the advection of voluminous magmas has the potential to raise temperatures in the middle crust very quickly. Although pluton-related thermal signatures significantly dissipate within <10 Myr (even for very large, high-temperature intrusive bodies), the interaction of pluton- and mantle-related thermal effects has the potential to maintain host rock temperatures in excess of 400–450 °C for up to 30 Myr in some parts of the mid-crust. The numerical models presented here support the notion that transient mantle-related heat sources have the capacity to contribute significantly to the thermal budget of metamorphism in high-*T*, low-*P* metamorphic belts, especially in those characterised by low surface heat flow, very high peak metamorphic geothermal gradients and abundant mafic intrusions.

Key words: Halls Creek Orogen; high-*T* low-*P* metamorphism; plutonism; thermal modelling.

INTRODUCTION

The formation of regionally extensive high-*T*, low-*P* metamorphic rocks ($T \geq 600$ °C, $P \geq 500$ MPa) fundamentally requires transient elevation of the geotherm (to values exceeding 35 °C km^{-1}) in the upper and middle section of the crust. In many high-*T*, low-*P* metamorphic belts, the heat source required is derived directly from within the crust, with heat transfer occurring (i) via conductive dissipation following voluminous mid-crustal plutonism (e.g. Lux *et al.*, 1986; Hanson & Barton, 1989), or (ii) via advection following the accretion of material with high radiogenic heat production at the base of the crust during continental collision (e.g. Ruppel & Hodges, 1994; Huerta *et al.*, 1998; Jamieson *et al.*, 1998). However, a large number of low *P*/*T*-ratio metamorphic terranes are characterised by a combination of first-order geological and thermal features inconsistent with a crustally derived heat source. These include (i) below-average surface heat flow; (ii) high-*T*, low-*P* metamorphic rocks cropping out continuously over a wide area; and, (iii) evidence for a prolonged thermal event, of the order of tens of millions of years in duration, during which the rocks cooled slowly at depth. Miyashiro (1973) was among the first to recognise the potential of additional heat input from the mantle as a mechanism capable of significantly elevating temperatures in the middle crust. Subsequent studies showed that heat flow from the mantle into the base

of the crust was significantly increased by physical processes which resulted in the attenuation or removal of the mantle lithosphere, such as delamination, detachment or convective thinning following crustal thickening (e.g. Bird, 1979; Houseman *et al.*, 1981; Wickham & Oxburgh, 1987; Loosveld & Etheridge, 1990).

This paper aims to evaluate the potential role of transient, mantle-related heat sources as a mechanism for high-T, low-P metamorphism in the middle crust, with specific reference to the Palaeoproterozoic (1915–1800 Ma) Halls Creek Orogen in north-western Australia. This terrane represents the collisional interface between the Kimberley and North Australian cratons, and contains areally extensive, prograde andalusite-sillimanite facies rocks with peak metamorphic $T = 700$–750 °C and $P = 400$–500 MPa (Thornett, 1986; Oliver & Barr, 1997; Bodorkos *et al.*, 1999; Oliver *et al.*, 1999). Specific geological and thermal properties of the orogen that support the operation of transient thermal anomalies in the mantle and/or preclude other obvious heat sources include:

(i) voluminous pre- to syn-metamorphic felsic plutons that do not show any systematic temporal or spatial association with the highest-grade metamorphic rocks;
(ii) field, petrologic and isotopic evidence for a protracted thermal event affecting the high-grade mid-crustal section exposed, with temperatures probably remaining above 400 °C for 30 Myr (Bodorkos *et al.*, 1999);
(iii) the recognition of over 40 layered mafic-ultramafic intrusions, emplaced at various crustal levels over a 30–40 million-year interval straddling the thermal peak of metamorphism (Hoatson, 1997);
(iv) low surface heat flow (< 50 mW m^{-2}) over the exposed area of the orogen (Fig. 1, see also Cull, 1982).

This combination of geological and thermal properties is difficult to explain in terms of a primarily crustally derived heat source such as mid-crustal plutonism or radiogenic heating. For example, although the accretion of high heat-producing material at the base of the deforming crust during continental collision is capable of triggering high-T, low-P metamorphism in the middle crust (e.g. Ruppel & Hodges, 1994; Huerta *et al.*, 1996; Batt & Braun, 1997; Huerta *et al.*, 1998; Jamieson *et al.*, 1998), the process is inevitably accompanied by a dramatic increase in the concentration of heat-producing elements at depth. Crustal material may contribute up to 120 mW m^{-2} to the syn-orogenic surface heat flow (Huerta *et al.*, 1996), and even after post-collisional erosion and the secular decline in the concentration of radionuclides in the crust, present-day surface heat flow in such provinces will exceed those of 'average' continental crust (in which crustal sources typically account for approximately 30–40 mW m^{-2} of the surface heat flow, Sclater *et al.*, 1980; Nyblade & Pollack, 1993). Thus, the radiogenic heating model is unlikely to be applicable to high-T, low-P metamorphic

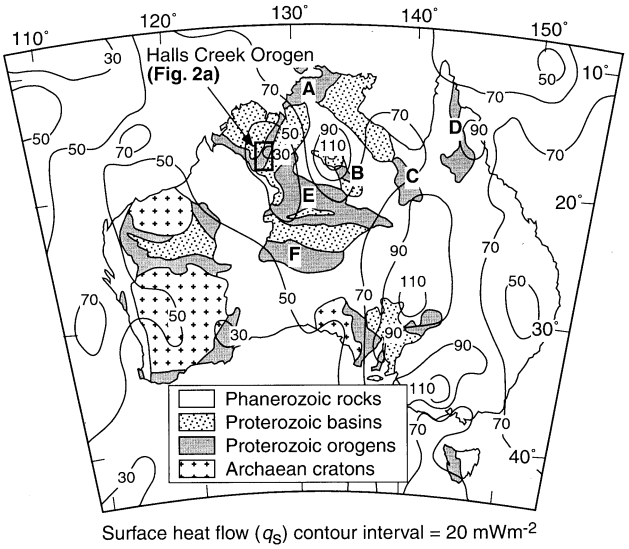

Fig. 1. Precambrian tectonic elements of Australia with contoured surface heat flow (q_s) data (modified from Cull, 1982). Proterozoic orogenic domains in northern and central Australia: A = Pine Creek, B = Tennant Creek, C = Mount Isa, D = Georgetown-Coen, E = Arunta, F = Musgrave (after Myers *et al.*, 1996). Measured q_s values exceed 70 mW m^{-2} over most Proterozoic orogens in northern Australia (e.g. A–D), and the Halls Creek Orogen is a notable exception in that $q_s = 30$–50 mW m^{-2} over its entire exposed area.

belts such as the Halls Creek Orogen, which are characterised by low present-day surface heat flow values.

Similarly, close temporal and spatial relationships between mid-crustal plutonism and zones of high-grade metamorphism are well-documented in many terranes (e.g. Lux *et al.*, 1986; Barton & Hanson, 1989; Sandiford *et al.*, 1991; Sandiford & Powell, 1991). However, metamorphism driven by magma advection is typically localised, transient and strongly dependent on the size of the intrusion and the magma–host rock temperature contrast (Hanson & Barton, 1989; De Yoreo *et al.*, 1991). Associated metamorphic terranes will therefore be characterised by high lateral metamorphic field gradients (several tens of °C km^{-1}, Sonder & Chamberlain, 1992) in the vicinity of intrusions, and heating-cooling cycles of short duration.

In this paper, we summarise the metamorphic evolution of the Palaeoproterozoic Halls Creek Orogen, and contrast the geology and thermal properties of this crustal segment with orogenic domains of similar age elsewhere in northern Australia. We outline a conceptual model in which high-T, low-P metamorphism in the Halls Creek Orogen is triggered by a transient, mantle-related heat pulse applied to the base of a crust with largely uniform and time-invariant physical and thermal properties. The heat pulse is simulated numerically by temporarily elevating the temperature of the upper mantle lithosphere to that of the asthenosphere ($\simeq 1300$ °C), and the thermal

response of the middle crust is evaluated. Parameters defining the physical properties of the model crust are assessed in terms of their control on the thermal evolution, and the model is extended by considering the interaction between crustal heating attributable to the conductive dissipation of the mantle-related heat pulse and 'regional contact' metamorphism resulting from plutonism that is likely to accompany it. Finally, the model results are compared with data constraining the thermal evolution of the Halls Creek Orogen.

SURFACE HEAT FLOW AND PROTEROZOIC HIGH-*T*, LOW-*P* METAMORPHISM IN NORTHERN AUSTRALIA

The majority of Proterozoic orogenic domains within the North Australian Craton are characterised by relatively high surface heat flow, with average values exceeding 70 mW m^{-2} (locally up to 110 mW m^{-2}) over the exposed areas of the Pine Creek, Tennant Creek, Mount Isa and Georgetown-Coen inliers (A–D in Fig. 1, see also Myers *et al*., 1996). The surface heat flow data summarised in Fig. 1 is based on the compilation of Cull (1982), which includes 35 heat flow measurements from Australian Proterozoic terranes with an average value of 85 mW m^{-2} (Sandiford & Hand, 1998). These elevated values are directly attributable to the widespread presence of voluminous felsic intrusions with high concentrations of heat-producing elements (e.g. granitic rocks in the Mount Isa Inlier have an average volumetric heat production of 5 μW m^{-3} and peak at 10 μW m^{-3}, McLaren *et al*., 1999). Deep seismic tomography suggests that the lithosphere is 250 km thick beneath north-eastern Australia (Zielhuis & van der Hilst, 1996), consistent with a present-day background mantle heat flux of *c.* 15–20 mW m^{-2} (Sandiford & Hand, 1998) which in turn suggests that at least 60–65 mW m^{-2} of the surface heat flow is due to crustal heat sources. Sandiford & Hand (1998) showed that high-*T*, low-*P* metamorphism may occur in the absence of significant contemporaneous plutonism, when a layer with anomalously high heat production is buried to mid-crustal depths.

In contrast, surface heat flow in the Halls Creek Orogen is <50 mW m^{-2}, which is comparable to that of the areally extensive Arunta and Musgrave inliers in central Australia (E and F in Fig. 1). All three terranes are characterised by the presence of large volumes of low heat-producing mafic and ultramafic rocks. In the Halls Creek Orogen, over 40 layered mafic-ultramafic intrusions have been recognised and mapped, and the largest of these has an estimated thickness of 7.8 km and an exposed area of 84 km^2 (Hoatson, 1997; Sproule *et al*., 1999). It is likely that the locus of deep crustal mafic plutonism is defined by a linear belt of large positive gravity anomalies that coincides with the axis of the orogen (Mathur & Shaw, 1982).

Deconvolving the surface heat flow into its mantle- and crust-related components, it is apparent that even if the background mantle heat flux is low ($<$15–20 mW m^{-2}), the total present-day crustally derived heat flow cannot exceed 35 mW m^{-2}, which is less than half that of some other Proterozoic orogenic domains in northern Australia. Consequently, even allowing for the removal of heat-producing material during erosion of the rocks above the current level of exposure, crustal radiogenic heating is precluded as the primary heat source for high-*T*, low-*P* metamorphism in the Halls Creek Orogen.

REGIONAL GEOLOGY OF THE HALLS CREEK OROGEN

Overview

The Halls Creek Orogen (Fig. 2a), comprises three tectono-metamorphic zones (Western, Central and Eastern) with discrete histories of sedimentation, deformation, metamorphism and intrusive activity constrained by U-Pb SHRIMP zircon data (Page *et al*., 1995a, 1995b; Tyler *et al*., 1995, 1999; Griffin *et al*., 2000). The Western and Central zones correspond to proximal and distal parts of the Kimberley Craton margin, respectively, and the Eastern zone represents the passive margin of the North Australian Craton.

The early tectonic evolution of the Kimberley Craton margin remains poorly understood, primarily due to the absence in the Western and Central zones of 'basement' rocks that significantly predate the first thermal event recognised (Sheppard *et al*., 1999; Tyler *et al*., 1999; Bodorkos *et al*., 2000b; Griffin *et al*., 2000). In the Western zone, the oldest rocks exposed are turbiditic sedimentary sequences of the Marboo Formation, which were deposited rapidly in the interval 1870–1865 Ma. Widespread low- to medium grade metamorphism (and restricted high-*T*, low-*P* metamorphism) at 1861 ± 5 Ma (Tyler *et al*., 1999) is spatially and temporally associated with voluminous, high-K felsic plutons emplaced into the sequence over the interval 1865–1850 Ma (Sheppard *et al*., 1995). These granites are restricted to the Western zone, and Griffin *et al*. (2000) inferred a 'post-collisional' tectonic setting, based on their geochemical similarity to the Phanerozoic pre-Cordilleran granites of South America. This interpretation requires the accretion of an 'exotic' (and currently unexposed) terrane to the eastern margin of the Kimberley Craton at *c.* 1900 Ma. Griffin *et al*. (2000) suggested that the collisional remnants are concealed below the post-1830 Ma Kimberley Basin succession of the Western zone (Fig. 2a), based on the existence of deep-seated linear gravity and magnetic highs in this region (Gunn & Meixner, 1998).

In the Central zone, siliciclastic units of the supracrustal Tickalara Metamorphics contain detrital zircon as young as *c.* 1865 Ma (Page *et al*., 1995a; Bodorkos *et al*., 2000b). These rocks are intruded by several large layered mafic-ultramafic intrusions with U-Pb SHRIMP zircon ages in the range 1860–1855 Ma (Hoatson & Tyler, 1993; Page *et al*., 1995a; Hoatson, 1997), and a suite of smaller mafic plutons synchronous with high-*T*, low-*P* metamorphism at 1845 ± 4 Ma (Bodorkos *et al*., 1999; Oliver *et al*., 1999). The oldest post-metamorphic granitoids intruded the Central zone at *c.* 1835 Ma, and are characterised by intermediate compositions and trace-element geochemistry reminiscent of Phanerozoic subduction-related granites (Sheppard *et al*., 1997), prior to a collisional event at *c.* 1820 Ma which juxtaposed the amalgamated Western and Central zones against the weakly deformed, 1915–1845 Ma passive-margin sedimentary sequences of the Eastern zone (Fig. 2a). Post-1820 Ma granites intrude and 'stitch' the southern part of the Angelo-Halls Creek Fault system between the Central and Eastern zones. In addition, basal units of the Kimberley Group sedimentary succession overlapping all three zones have been dated at *c.* 1800 Ma (Tyler *et al*., 1995).

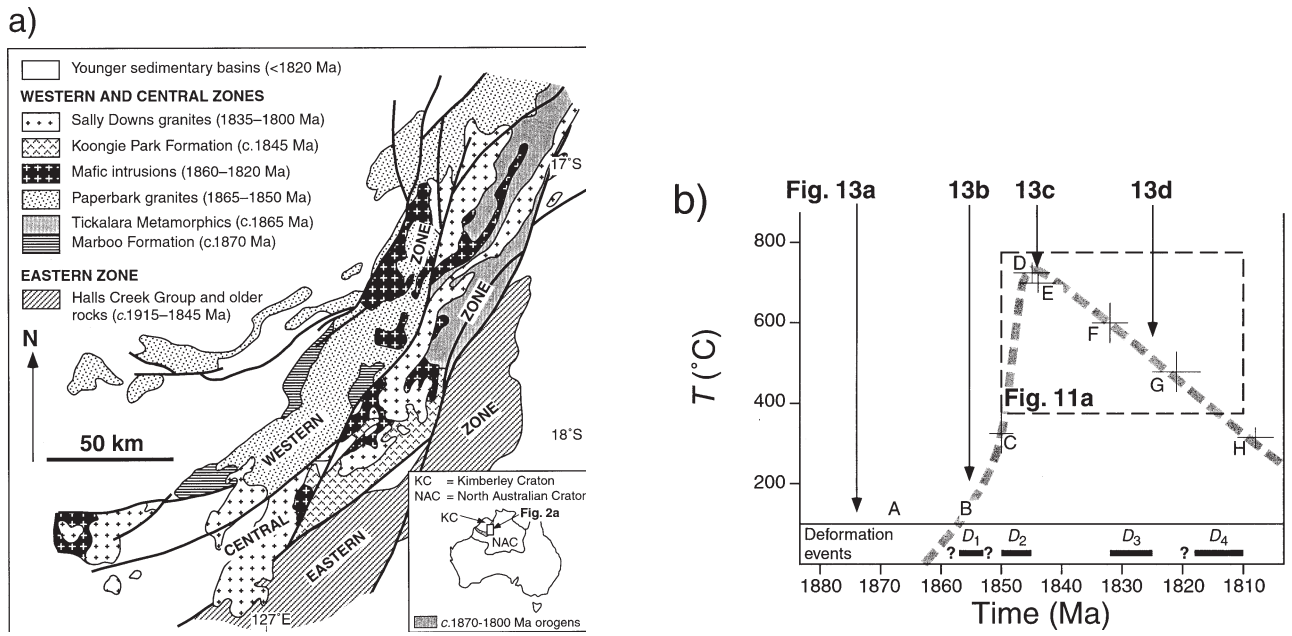

Fig. 2. Major Palaeoproterozoic geological elements of the Halls Creek Orogen, which represents the interface of the 1860–1800 Ma collision between the Kimberley (west) and North Australian (east) cratons. (b) *T–t* curve for the mid-crustal Tickalara Metamorphics in the northern central Halls Creek Orogen. A full description of the constraints on the points A–H is given in Table 1.

Thermal history of the Central zone

The high-*T*, low-*P* rocks of the Tickalara Metamorphics in the northern Central zone underwent a thermal event that differs in several important respects to that preserved by rocks in the Western zone. In the Western zone, the thermal peak of metamorphism occurred at 1861 ± 5 Ma (Tyler *et al*., 1999), and the high-*T*, low-*P* rocks display a close temporal and spatial relationship with abundant and voluminous 1865–1850 Ma granites (see fig. 2 of Tyler *et al*., 1999). In contrast, granulite-facies high-*T*, low-*P* metamorphic rocks crop out extensively (strike length > 50 km) in the northern part of the Central zone, despite the complete absence of the 1865–1850 Ma granites that dominate exposure in the Western zone. Furthermore, no spatial relationship exists between regional metamorphic grade and the suites of layered mafic-ultramafic plutons in the Central zone, the majority of which were emplaced during the intervals 1860–1855 Ma and 1830–1820 Ma (Page *et al*., 1995a), temporally straddling the thermal peak of metamorphism at 1845 ± 4 Ma (Bodorkos *et al*., 2000b). The largest mafic intrusions are the pre-metamorphic 1856 ± 2 Ma Panton suite and the post-metamorphic 1830 ± 3 Ma McIntosh pluton, both of which intrude relatively low-grade, unmelted Tickalara metasedimentary rocks in the centre of the Central zone (Hoatson, 1993; Page *et al*., 1995a; Hoatson, 1997). Broadly syn-metamorphic mafic plutons (such as the 1841 ± 3 Ma Sally Malay pluton, Trudu & Hoatson, 1996) intruding the high-grade rocks of the northern Central zone are relatively small and rare (Hoatson, 1997).

Rocks of the Central zone also preserve evidence of a protracted thermal event in the middle crust. Field, petrological and isotopic data constraining the *T–t* evolution of this area are described in detail in Bodorkos *et al*. (1999), and briefly summarised here in Fig. 2(b) and Table 1. Regional D2 deformation was broadly synchronous with high-*T*, low-*P* metamorphism in the Tickalara Metamorphics at *c.* 1845 Ma, and the S2 fabric in these rocks is overprinted by another two macroscopic deformation events (D3 and D4, see Bodorkos *et al*., 1999) in the ensuing 30–40 Myr. The syn-D3 deformation regime was dominated by the development of ductile structures synchronous with emplacement of the 1832 ± 3 Ma Mabel Downs Tonalite (Page *et al*., 1995b) under amphibolite facies conditions, some 10–15 Myr after the thermal peak of regional metamorphism (Fig. 2b, see also Bodorkos *et al*., 2000a). Coeval mafic plutons intruding high-grade metapelites are characterised by the development of thick 'sheath' leucosomes and extensive back-veining along their cuspate margins, relationships consistent with pluton emplacement into hot host rocks (Oliver & Barr, 1997). The oldest brittle-regime structures are faults which post-date an *c.* 1820 Ma granitoid and truncate the limbs of macroscopic D4 folds, suggesting that temperatures remained above 400 °C over the interval 1845–1815 Ma (Fig. 2b, see also Table 1).

The relatively long-lived nature of the thermal event in the Central zone, and the absence of a one-to-one spatial association between exposed plutons and the distribution of metamorphic isograds precludes advection of heat from the lower crust in melts as the primary source of heat for high-*T*, low-*P* metamorphism in the Central zone. This combination of features is more consistent with conductive heating resulting from a transiently perturbed thermal regime in the upper mantle, a scenario entirely consistent with the temporal association between mantle-derived mafic-ultramafic plutonism, deformation and high-grade metamorphism.

MANTLE-RELATED CRUSTAL HEATING

Conceptual models and their application to the Halls Creek Orogen

The thermal problem we wish to investigate is analogous to any situation in which the temperature of the upper mantle is transiently elevated, such that the conductive heat flux through the base of the crust exceeds the heat flow supplied to the base of the lithosphere by the deeper mantle. Most of the physical

Table 1. Summary of data constraining the thermal evolution of the central Halls Creek Orogen as depicted in Fig. 2(b). All errors are quoted at the 95% confidence level.

Point (Fig. 2b)	Age (U-Pb SHRIMP zircon unless otherwise specified)	*P-T* estimate and/or geological interpretation
A	1865±2 Ma (Page *et al*., 1995a) 1864±4 Ma, 1867±4 Ma (Bodorkos *et al*., 2000b)	Detrital zircons placing an older limit on the depositional age of the protoliths to the northern Tickalara metasedimentary units
B	1857±2 Ma, 1856±2 Ma, 1855±2 Ma (Hoatson, 1997; Page *et al*., 1995a)	Ages of the Springvale, Panton and Toby layered mafic-ultramafic intrusions
C	1850±2 Ma (Page *et al*., 1995b)	Emplacement of the garnet-bearing leucocratic Fletcher Creek Granite ($T \simeq 700$ °C) into cold host rocks ($T < 400$ °C), producing a prominent metamorphic aureole
D	1845±4 Ma (Bodorkos *et al*., 2000b) 1845±3* Ma (Oliver *et al*., 1999)	Peak metamorphism ($T \simeq 700 \pm 50$ °C, $P \simeq 400$ MPa) in Tickalara pelitic gneisses and migmatites
E	1844±3 Ma (Hoatson, 1997)	Discordant emplacement of the Sally Malay layered mafic intrusion post-dating peak metamorphism, remelting stromatic migmatites of the Tickalara Metamorphics
F	1832±3 Ma (Page *et al*., 1995b) 1833±3 Ma (Bodorkos *et al*., 2000a)	Emplacement of the Mabel Downs Tonalite during ductile *D*3 deformation ($P > 300$ MPa) and amphibolite facies metamorphism ($T > 500$ °C)
G	1821±4 Ma (Sheppard *et al*., 1995)	Emplacement of the broadly syn-*D*4 Sally Downs Tonalite, which contains large-scale *F*4 folds with limbs truncated by brittle *S*4 fault and shear zones ($T < 400$ °C, $P \simeq 300$ MPa)
H	1808±3 Ma (Sheppard *et al*., 1995)	Emplacement of the Mount Christine Granitoid in the southern Halls Creek Orogen, 'stitching' a major late-stage brittle *S*4 fault ($T < 400$ °C, $P < 300$ MPa)

*conventional U-Pb monazite age.

processes capable of raising temperatures in the upper mantle involve upwelling of hot asthenospheric material following attenuation or removal of the mantle lithosphere via convective thinning (e.g. Houseman *et al*., 1981; Loosveld & Etheridge, 1990), delamination (e.g. Bird, 1979; Sacks & Secor, 1990), detachment via 'slab breakoff' (e.g. Davies & von Blanckenburg, 1995), or extension (Sandiford & Powell, 1986) either preceding or post-dating shortening (Thompson, 1989; Houseman & Molnar, 1997). Attenuation of the mantle lithosphere is often accompanied by decompression melting and the emplacement of mantle-derived mafic magmas at the base of the crust as an underplate (e.g. Wells, 1980; Ellis, 1987; Etheridge *et al*., 1987). All of these scenarios may be considered as providing a transient thermal 'pulse', with respect to the thermal evolution of the overlying crust. Heat input occurs via conductive dissipation, and advection, either directly through the emplacement of mantle-derived mafic-ultramafic plutons in the middle crust, or indirectly via the ascent of granitic magmas generated as a consequence of partial melting in the lower crust.

In the Halls Creek Orogen, existing models for the tectonic evolution of the region invoke elevated temperatures in the upper mantle as the primary heat source for metamorphism. Griffin *et al*. (2000) suggested that accretion of an exotic (and now unexposed) continental fragment along the eastern margin of the Kimberley Craton at 1900–1880 Ma was preceded by subduction of the intervening oceanic crust beneath the Kimberley Craton. In this model, collision was accompanied by deposition of the Marboo Formation in the Western zone and the protoliths to the Tickalara Metamorphics in the Central zone, and followed by collapse of the subducting slab and delamination of the mantle lithosphere. This combination of processes resulted in upwelling of hot asthenospheric material beneath the crust of the Western and Central zones (fig. 14 of Griffin *et al*., 2000), triggering plutonism and metamorphism in the middle crust. In the following section, we develop a generalised numerical model to describe this conceptual scenario.

Modelling a mantle-related thermal pulse

We are interested in simulating a transient thermal anomaly in the upper mantle and evaluating the thermal response of the crust at depths appropriate to the widespread low-*P* metamorphism observed in the Halls Creek Orogen. Consequently, our model focuses on establishing the likely magnitude, timing and duration of temperature increases in the middle crust that are directly attributable to a mantle temperature anomaly, and initially neglects the thermal effects of 'intracrustal' processes such as plutonism and the vertical redistribution of radiogenic heat production. We describe the physical and thermal properties of the model crust, before focusing on the theory of our mantle-related temperature anomaly.

Properties of the model crust

The simplified model crust is two-dimensional (x = horizontal width, z = depth) with uniform and time-invariant thickness (z_c) and thermal conductivity (k), and within which heat is transported by conduction (variables and values used are summarised in Table 2). Other physical and thermal properties are constrained by geological data from the Halls Creek Orogen, where the crustal contribution to the present-day surface heat flow is 15–35 mW m^{-2} (based on a total surface heat flow of 30–50 mW m^{-2} which includes a reduced mantle heat flow contribution of at least 15–20 mW m^{-2}, Sandiford & Hand, 1998). Taking into account the secular decline in the concentration of radionuclides in the crust since *c.* 1800 Ma, the contribution of the preserved crustal section to the surface heat flow during the Early Proterozoic was 20–45 mW m^{-2}, although this represents a lower limit on the syn-metamorphic crustal heat production in view of the subsequent removal of upper crustal material through erosion. The crust currently exposed in the Halls Creek Orogen is relatively unradiogenic, with an area-averaged volumetric heat production of approximately 2.25 μW m^{-3} based on the outcrop proportions, whole-rock chemistry and density of the principal rock units exposed (see Table 3). Recalculating radionuclide concentrations in these rocks to 1800 Ma yields an area-averaged volumetric heat production of 3.2 μW m^{-3} for the crustal level currently exposed (Table 3). We use this value as the volumetric heat production at the Earth's surface

(H_0) with respect to our model crust, and reproduce the present-day surface heat flow by assuming a standard distribution in which the concentration of heat producing elements decreases exponentially with depth, with a characteristic vertical length scale $z_r = 10$ km (such that $H(z_r) = H_0/e$).

Mantle temperature anomaly—theory and analytical solution

We simulate a thermal anomaly in the upper mantle by setting temperature $T = T_a$ (the temperature of the asthenosphere; see Table 2) at time $t = 0$ for depth $z = z_D$ (the 'depth to anomaly'), and maintaining $T = T_a$ in this lithospheric section over the time interval $0 < t < t_D$. The long-term ($t \geq t_D$) thermal evolution of this scenario is well understood by analogy with cooling of newly formed oceanic lithosphere at a mid-ocean ridge (e.g. McKenzie, 1967; Sleep, 1969; Sclater *et al.*, 1971; Lubimova & Nikitina, 1975), which corresponds to the special case $z_D = 0$ km. For a two-dimensional lithospheric plate with thickness L, no radiogenic heat production, $T = 0$ °C at the top of the plate ($z = 0$), and constant temperature $T = T_a$ at the ridge axis ($x = 0$) and the base of the plate ($z = L$), the equation governing T is:

$$\kappa\left(\frac{\partial^2 T}{\partial x^2} + \frac{\partial^2 T}{\partial z^2}\right) = u\frac{\partial T}{\partial x} \quad (1)$$

Table 2. Definitions of variables and values used.

Variable	Definition	Value/Units	Comment
x	horizontal distance	km	$x = 0$ is the vertical axis of the mantle-related temperature anomaly
z	vertical distance	km	$z = 0$ at the Earth's surface; positive downwards
z_c	vertical thickness of the model crust	km	
k	thermal conductivity	W m^{-1} °C^{-1}	time- and depth-independent throughout the model crust
H_0	volumetric heat production at the Earth's surface in the model crust	3.2 μW m^{-3}	
z_r	vertical length scale of heat production distribution in the model crust	km	$H(z_r) = H_0/e$
T	temperature		
T_a	temperature at the base of the lithosphere	1300 °C	
t	time	Ma	mantle-related temperature anomaly is initiated at $t = 0$
z_D	minimum thickness of the thinned lithosphere	km	depends on x; z_D is minimised at $x = 0$
t_D	duration of the interval over which $T \approx T_a$ is maintained in the specified lithospheric domain	Ma	
L	vertical thickness of lithospheric plate	150 km	
κ	thermal diffusivity	10^{-6} m^2 s^{-1}	
T_b	background (*time-invariant*) component of the temperature field	°C	depends only on z in a model crust with specific thermal properties
T_{anom}	additional (*transient*) component of the temperature field	°C	depends on z, t and x
k^*	'anomalous' thermal conductivity	W m^{-1} °C^{-1}	$k^* = 10^3$k in the interval $0 \leq t \leq t_D$
x_r	horizontal length scale (half-width) of mantle-related temperature anomaly	km	$T(x_r) = T(x = 0)/\sqrt{e}$
ΔT	temperature increase associated with any thermal perturbation	°C	$\Delta T = T_{anom}$ for mantle-related thermal pulse
T_{max}	maximum temperature attained at specified point in crust	°C	
ΔT_{max}	maximum value of the temperature increase associated with any thermal perturbation	°C	$\Delta T_{max} = T_{max} - T_b$
$\partial T/\partial t$	cooling rate following attainment of ΔT_{max}	°C Ma^{-1}	
$t(\Delta T_{max})$	time at which ΔT_{max} occurs	Ma	
ΔT_{half}	half the maximum temperature increase associated with any thermal perturbation	°C	$\Delta T_{half} = \Delta T_{max}/2$
$t(\Delta T_{half})$	time at which ΔT_{half} occurs	Ma	$t(\Delta T_{half}) > t(\Delta T_{max})$
$(\partial T/\partial t)_{mean}$	average cooling rate over the time interval required for ΔT_{max} to decay to ΔT_{half}	°C Ma^{-1}	$(\partial T/\partial t)_{mean} = \frac{\Delta T_{max} - \Delta T_{half}}{t(\Delta T_{max}) - t(\Delta T_{half})}$
T_i	temperature of mafic intrusion	°C	
x_i	horizontal half-width of mafic intrusion	km	
z_i	vertical thickness of mafic intrusion	km	

Table 3. Common rock types in the northern Halls Creek Orogen and their volumetric heat production values, based on measured concentrations of K, U and Th from Sheppard *et al.* (1995) and S. Bodorkos (unpublished data). Present-day heat production for each rock type is calculated, and the weighted average recast to 1800 Ma using equations 4–6 and 4–8 of Turcotte & Schubert (1982, p. 140).

Map unit	Rock type	Heat production H (μ Wm^{-3})	Outcrop area in northern central Halls Creek Orogen (% of total)
Paperbark Supersuite	granites, felsic volcanic rocks	3.27	35
	mafic rocks	0.88	10
Tickalara Metamorphics	clastic metasedimentary rocks	1.69	20
Sally Downs Supersuite	granitic rocks	2.57	24
	mafic rocks	0.26	6
Mabel Downs Suite	granitic rocks	1.46	4
	mafic rocks	0.79	1
Mean H (weighted by present-day outcrop area)		2.25	100
Mean H recalculated to 1800 Ma		3.19	

In eq. (1), u is the horizontal velocity of the plate and the term on the right-hand side is due to advection of heat with the moving plate (Sleep, 1975; Morton & Sleep, 1985; Fowler, 1990). Setting time $t = x/u$, the solution given by Fowler (1990) to eq. (1) using the initial and boundary conditions stated above is:

$$T = T_a\left(\frac{z}{L} + \sum_{n=1}^{\infty}\frac{2}{n\pi}\sin\left[\frac{n\pi z}{L}\right]\exp\left[\frac{ut}{L}\left(\frac{uL}{2\kappa} - \sqrt{\frac{u^2L^2}{4\kappa^2} + n^2\pi^2}\right)\right]\right) \quad (2)$$

Assuming that the horizontal conduction of heat is insignificant in comparison to the horizontal advection and vertical conduction of heat (2) simplifies to:

$$T = T_a\left(\frac{z}{L} + \sum_{n=1}^{\infty}\frac{2}{n\pi}\sin\left[\frac{n\pi z}{L}\right]\exp\left[-\frac{n^2\pi^2\kappa t}{L^2}\right]\right) \quad (3)$$

This expression has the form:

$$T(z, t) = T_b(z) + T_{anom}(z, t) \quad (4)$$

where $T_b(z)$ and $T_{anom}(z, t)$ are the time-invariant and transient components, respectively, of the temperature field.

Mantle temperature anomaly—numerical simulation

We seek to model the transient thermal perturbation experienced by a lithospheric section with uniform and time-invariant thickness z_D ($z_D \geq z_c$), following the instantaneous elevation of temperatures in the underlying mantle lithosphere such that $T \approx T_a$ for $z \geq z_D$ and $0 < t < t_D$. This is implemented using a finite-element algorithm which artificially adjusts the thermal conductivity k within the lithospheric domain that is removed. Using the boundary conditions of the two-dimensional plate model ($T = 0$ °C at $z = 0$, $T = T_a$ at $x = 0$ and $z = L$), we utilise the idea that in a conductive regime, an increase in k of several orders of magnitude within a specified domain results in the almost instantaneous homogenisation of the temperature field in that domain. Consequently, we generate a thermal anomaly in the lithosphere by setting $k^* = 10^3 k$ within a restricted lithospheric domain for the interval of time $0 < t < t_D$, corresponding to the interval over which the mantle anomaly is dynamically maintained. At $t = t_D$, k is reset to its correct value, with the result that the thermal anomaly decays back to the initial condition with a characteristic time-scale governed by the thickness and thermal diffusivity of the lithosphere. Figure 3 shows the thermal evolution of the model lithosphere at $x = 0$ for $z_D = 0$ and time $t > t_D$, analogous to cooling and thickening of the lithosphere at a mid-ocean ridge following cessation of rifting at $t = t_D$. Superimposed on the curves (which represent the model geothermal gradient at each time-step) are unfilled circles which represent the solutions to eq. (3) for the applicable z and t. The temperatures obtained from the numerical model are within 2 °C of the analytical solutions to eq. (3) throughout, showing that the thermal conductivity manipulation used in our model accurately reproduces the cooling history ($t \geq t_D$) of lithosphere for which $T = T_a$ over $z_D \leq z \leq L$ and $0 < t < t_D$.

The vertical and horizontal extent of the lithospheric domain in which $k = k^*$ for $0 < t < t_D$ is confined by the definition of $z_D(0)$ as the 'depth to anomaly' at $x = 0$ ($k = k^*$ for $0 < t < t_D$ over the depth interval $z_D(0) < z < L$), simulating the removal of a lithospheric section with thickness $L - z_D(0)$. The value of z_D increases (and the lithospheric thickness removed decreases) away from $x = 0$, with a horizontal length scale (or half-width) x_r such that:

$$z_D(x) = L - (L - z_D(0))\exp\left[-\left(\frac{x}{x_r}\right)^2\right] \quad (5)$$

This relationship represents a proxy for the model results of Sleep (1996), which suggest that lateral flow of hot asthenosphere may occur over hundreds of kilometres in response to pre-existing topographic variations at the lithosphere–asthenosphere boundary,

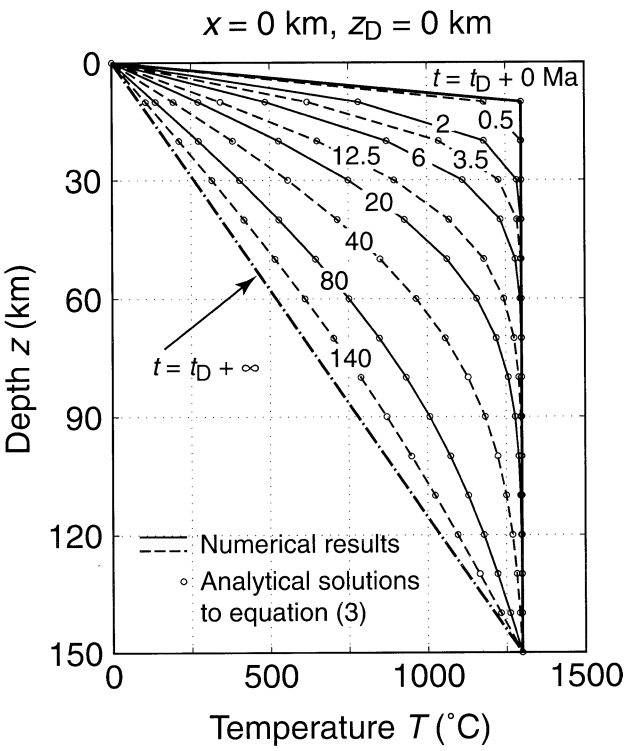

Fig. 3. Plot showing the evolution of geotherms (solid and dashed lines) derived from our numerical model, following the reimposition of background k in the lithosphere at $t = t_D$, for the special case $x = 0$ and $z_D(0) = 0$ km (approximating the thermal evolution of newly formed oceanic lithosphere at a mid-ocean ridge). Small circles represent analytical solutions to eq. (3) at the appropriate z and t, and model values show excellent agreement with analytical solutions (within 2 °C in all cases).

resulting in large-scale 'ponding' of buoyant plume-related material. Figure 4(a) illustrates the geometry of the model lithosphere for the case $z_D(0) = 40$ km, and the locations of stationary points in the overlying crust where thermal histories are calculated and assessed in the next section. Note that for simplicity, our model neglects the effects of uplift associated with thermal expansion accompanying lithospheric removal, i.e. L remains constant throughout. Figure 4(b) shows the thermal structure of the model lithosphere at $x = 0$ for $z_D(0) = 40$ km. The steady state geotherm (corresponding to $t = 0$ and $t \simeq t_D + \infty$) shown in the shaded upper portion of the lithosphere ($0 < z < z_D$) is dictated by the physical and thermal properties of the model crust. In the lower portion of the lithosphere ($z_D \leq z < L$), $T \simeq T_a$ throughout at $t = t_D$, with the thermal anomaly decaying until background temperatures are reattained at $t \simeq t_D + 100$ Ma.

In the following section, we investigate the effects of varying several parameters controlling the physical and thermal properties of the crust and mantle which also have the potential to exert significant influence on the thermal evolution of the model crust. Important mantle parameters include the intensity of the temperature anomaly (T_a), its vertical and horizontal extent (z_D and x_r), and the duration (t_D) for which it is dynamically maintained. In the crust, the thermal conductivity (k) and the distribution of heat-producing elements (z_r) are critical. Thermal histories predicted by our numerical model are presented as plots for selected points in the crust, showing time-dependent variations in temperature and/or cooling rate over a 100 million year interval, following the imposition of the temperature anomaly (i.e. setting $k = k^*$ in the specified domain) at $t = 0$. Following our initial evaluation of the thermal signature of such

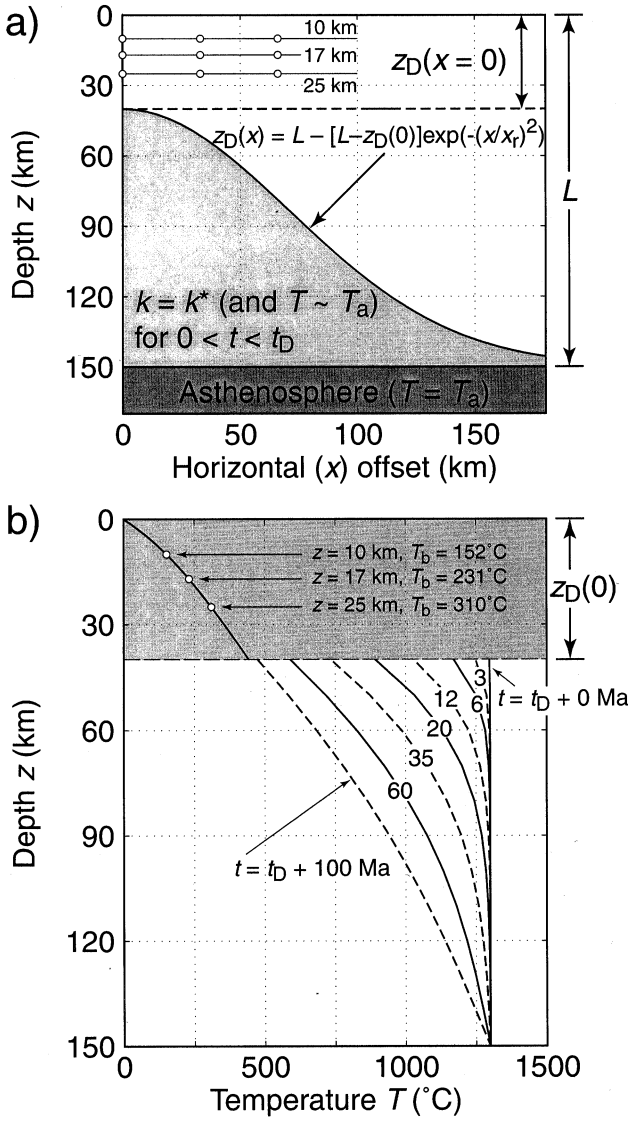

Fig. 4. (a) Geometry of the two-dimensional lithosphere used in the numerical model. The thermal conductivity k is increased to $k^* = 10^3 k$ within the lithospheric domain shaded light grey (confined vertically and horizontally by specified values of $z_D(x=0)$ and x_r, respectively), and dynamically maintained over the time interval $0 < t < t_D$. All model properties are reflected about $x=0$. In this diagram, $z_D(x=0) = 40$ km, $L = 150$ km and $x_r = 100$ km. Within the overlying lithosphere, the small circles at $x=0$, 33 and 66 km for $z=10$, 17 and 25 km are the locations of points for which ΔT–t curves are calculated. (b) Temperature-depth plot showing evolution of the lithosphere geotherms (solid and dashed lines) at $x=0$ when $z_D(0) = 40$ km, over 100 Myr following the reimposition of background k at $t = t_D$. The background geotherm in the lithospheric section $0 < z < z_D$ corresponds to a crust with $k = 3$ W m^{-1} °C^{-1} and an exponentially decreasing vertical distribution of heat production $H = H_0 \exp[-(z/z_r)]$, with $H_0 = 3.2$ μW m^{-3} and $z_r = 10$ km (see text).

an anomaly operating in isolation, we consider the possible thermal consequences of the emplacement of mafic magmas in the middle crust, as a likely lower-crustal and upper-mantle response to elevated mantle heat flow. Finally, we examine the interplay between the localised effects of such plutonism and the regional temperature anomaly in terms of the intensities and time-scales of the thermal pulses produced.

MODEL RESULTS AND DISCUSSION

The model presented above allows the assessment of the time- and space-dependent variations in transient mantle heat flux, applied beneath a crust which has fixed physical and thermal properties. Consequently, the thermal evolution of the crust is dictated by a thermal pulse that sweeps up through the crust and outwards from the locus of the anomaly (at $x=0$ in the two-dimensional model lithosphere). The amplitude of the temperature increase experienced by any point in the crust is defined as:

$$\Delta T = T_{anom} = T - T_b \qquad (6)$$

where T_b is the time-invariant background temperature. Figure 5 shows the calculated ΔT, its maximum value (ΔT_{max}) and the cooling rate ($\partial T/\partial t$) through time for the locations and model parameters used in Fig. 4 (crust with $k = 3$ W m^{-1} °C^{-1}; $H_0 = 3.2$ μW m^{-3}, $z_r = 10$ km and a mantle anomaly with $z_D(0) = 40$ km, $x_r = 100$ km, $t_D = 5$ Myr). At $x=0$, the amplitude of the thermal pulse at mid-crustal depths ranges from $\Delta T_{max} \simeq 130$ °C ($z=10$ km) to $\Delta T_{max} \simeq 370$ °C ($z=25$ km), achieved 6–11 Myr after initiation of the mantle temperature anomaly. Peak temperature and cooling rate data are given in Table 4. At $x=0$, the mean cooling rate $(\partial T/\partial t)_{mean}$ averaged over the time interval required for ΔT_{max} to decay to half its value (see Table 2 for definition) ranges from 2.3 °C Ma^{-1} at $z=10$ km to 7.2 °C Ma^{-1} at $z=25$ km.

Influence of crustal parameters: thermal conductivity k and distribution of radiogenic heat production z_r

The overall thermal effects of variations in the abundance and distribution of heat-producing elements (z_r) and thermal conductivity k are complex, as these parameters control the steady-state crustal geotherm as well as influencing the magnitude of the thermal pulse. Higher values of z_r elevate background crustal temperatures, and the steepened geotherm outweighs the associated decrease in the amplitude of ΔT, resulting in higher peak metamorphic temperatures in the crust at higher z_r (see Fig. 6a). Similarly, lower values of k elevate the background geotherm and result in higher peak temperatures, despite the fact that ΔT_{max} is both larger and more rapidly attained at higher k (Fig. 6b). Note that the vertical axes of the plots in Fig. 6 represent actual temperature T (rather than ΔT), showing the interplay between T_b and the amplitude of ΔT. In addition, the solid black T–t paths in each vertical pair of panels in Fig. 6 are identical, enabling the comparison of effects attributable to variations in k and z_r, respectively.

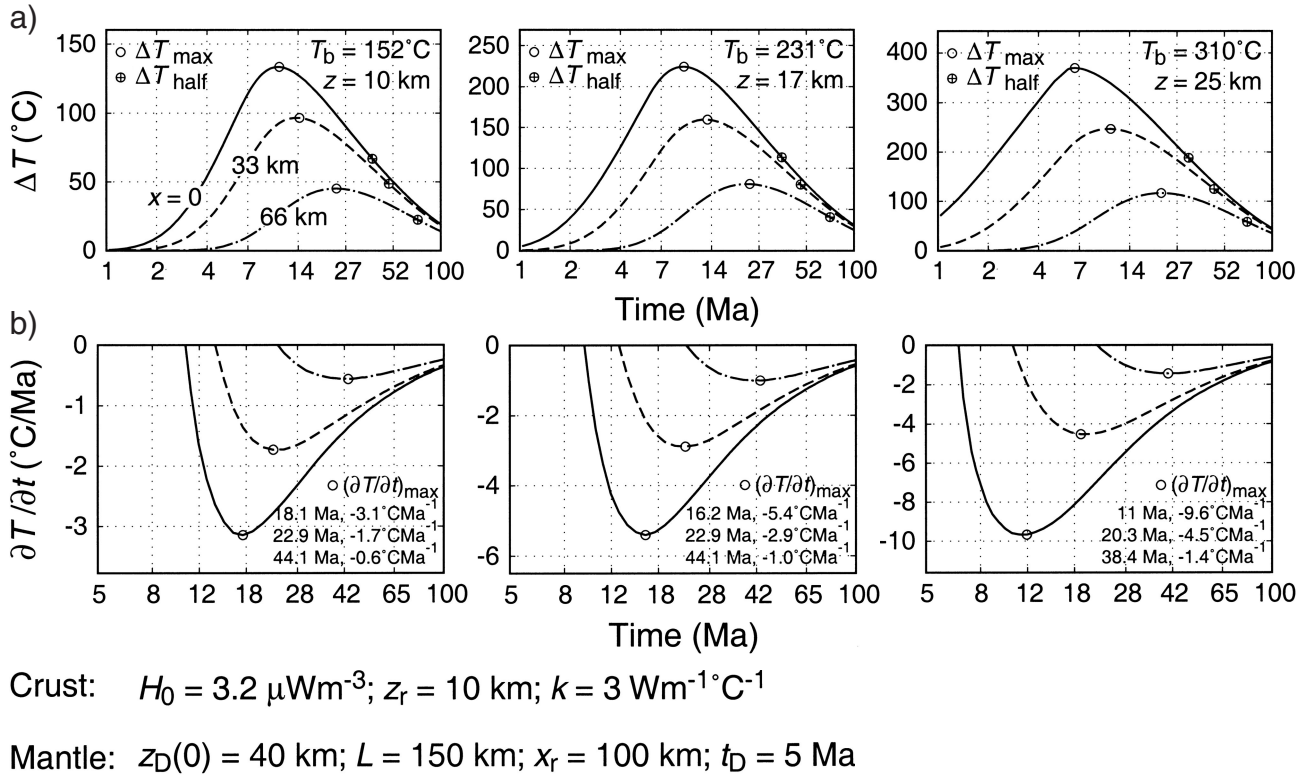

Fig. 5. Diagram showing ΔT–t (a) and cooling rate ($\partial T/\partial t$)–t curves (b) for each of the nine points shown in Fig. 4(a), using the model parameters specified. ΔT_{max}, ΔT_{half}, $t(\Delta T_{max})$ and $t(\Delta T_{half})$ data are given in Table 4. Maximum cooling rates and the times at which they are attained are shown within each panel.

Table 4. Values of ΔT_{max}, ΔT_{half}, $t(\Delta T_{max})$ and $t(\Delta T_{half})$ obtained for the model parameters specified in Fig. 4. See Fig. 5 for complete ΔT–t curves.

Depth z (km)	T_b (°C)		ΔT_{max} (°C)	$t(\Delta T_{max})$ (Ma)	ΔT_{half} (°C)	$t(\Delta T_{half})$ (Ma)	Time-averaged cooling rate $(\partial T/\partial t)_{mean}$ (°C Ma^{-1})
10	152	$x=0$ km	133.5	10.6	67.0	39.0	2.34
		$x=33$ km	96.7	13.8	48.3	49.3	1.36
		$x=66$ km	45.2	23.3	22.6	72.5	0.46
17	231	$x=0$ km	224.4	9.4	112.4	37.3	4.01
		$x=33$ km	159.7	12.8	79.7	48.3	2.25
		$x=66$ km	81.1	23.0	40.5	72.0	0.83
25	310	$x=0$ km	370.0	6.6	185.1	32.3	7.19
		$x=33$ km	246.9	10.6	123.8	45.3	3.54
		$x=66$ km	116.6	21.7	58.1	71.0	1.19

Influence of mantle anomaly parameters: depth z_D, half-width x_r and duration t_D

The focus of this study is on the thermal evolution of a fixed depth section of the crust ($z=10$–25 km) corresponding to a specific range of metamorphic pressures ($P=300$–700 MPa). It is intuitively obvious that magnitudes of ΔT_{max} experienced by this crustal section will increase for mantle-related temperature anomalies of larger horizontal extent (i.e. larger x_r) and/or longer duration (larger t_D), that are initiated at shallower depths in the lithosphere (smaller z_D), However, it is instructive to examine the relative sensitivity of the thermal evolution of the crust to each of these parameters, and Fig. 7 shows the influence of variations in z_D, t_D and x_r on ΔT–t curves for points at $x=0$ and $z=10$, 17 and 25 km. The solid black curves in each row of panels represent identical parameter values, for the purpose of comparison between adjacent plots.

Figure 7(a) shows that z_D exerts primary control on the amplitude of the thermal pulse experienced by the crustal section $z=10$–25 km at $x=0$ km, with significantly larger ΔT_{max} values attained much more quickly when $z_D=35$ km (followed by more rapid cooling), compared to the same region when $z_D=65$ km. When $z_D=40$ km, the magnitude of ΔT_{max} is more sensitive to variations in t_D than x_r over the range of values investigated; however, post-ΔT_{max} cooling rates are noticeably slower for higher values of x_r (Fig. 7b, c). The small across-strike thermal gradients associated with a temperature anomaly with large x_r allow temperatures along the anomaly axis to remain higher for longer, in comparison with a narrower anomaly with identical t_D.

Effects of large-scale mafic plutonism

Figure 7 shows that for large t_D and z_r (and/or small z_D), peak crustal temperatures close to the axis of

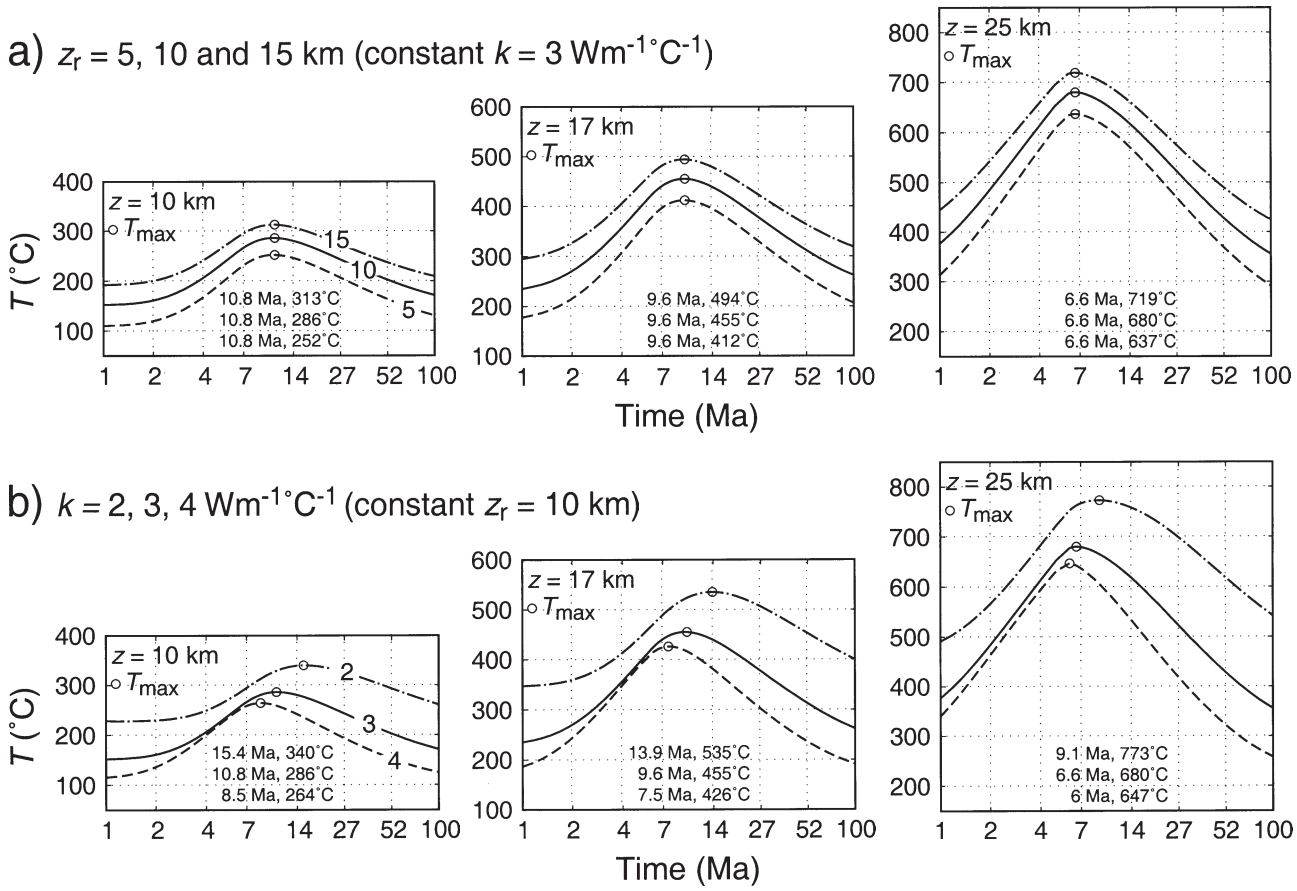

Fig. 6. *T–t* diagrams at $x=0$ for $z=10$, 17 and 25 km, showing the influence of variations in crustal parameters z_r and k. Note that the vertical axes of these plots are temperature T (rather than ΔT), as variations in k and z_r result in variations in the steady-state geotherm as well as the amplitude of ΔT. In addition, the solid black curves in each vertical pair of panels are identical, for the purpose of comparing the sensitivity of the *T–t* evolution to variations in each parameter. (a) *T–t* diagrams for $z_r=5$, 10 and 15 km at constant $k=3$ Wm^{-1} °C^{-1}. (b) *T–t* diagrams for $k=2$, 3 and 4 W m^{-1} °C^{-1} at constant $z_r=10$ km.

our mantle-related thermal anomaly (i.e. at $x\approx0$ km) will exceed 700–750 °C at $z=25$ km, and will be higher still in the deep crust. Large-scale crustal anatexis is a probable consequence of such heating, and mafic plutonism is also likely to accompany significant mantle-related heating of the crust via lithospheric removal and/or underplating. The segregation and ascent of such magmas clearly has the potential to further perturb thermal regimes in the overlying crust. In this section, we consider the thermal effects of a large mafic intrusion instantaneously emplaced in the middle crust ($T_i=1000$ °C, thickness $z_i=4$ km, half-width $x_i=30$ km; top surface $z=17.5$ km; see Fig. 8). First, we quantify the extent of temperature increases in the host rocks attributable solely to the conductive cooling of the intrusion (i.e. with no mantle heat pulse). We evaluate two possible end-member thermal scenarios for pluton emplacement: (i) $T_i=1000$ °C within the body of the intrusion only (approximating pluton emplacement via melt migration along a shear zone), and (ii) $T_i=1000$ °C within the sill and throughout the potential ascent path of the intrusion, as may be expected in diapir-style magma migration (Fig. 8). These two end-members bracket the probable thermal structure in the ascent path of a magmatic zone. Figure 9 shows the ΔT–t curves for each of these thermal scenarios at the points shown in Fig. 8(a), superimposed on the steady-state geotherm depicted in Fig. 8(b) in the absence of a mantle temperature anomaly.

As highlighted by many previous studies (e.g. Jaeger, 1959, 1964; Wells, 1980; Lux *et al.*, 1986; De Yoreo *et al.*, 1989; Hanson & Barton, 1989), the magnitude of the host rock temperature increase is a function of the initial temperature contrast between the magma and the host rock, and values of ΔT_{max} are significantly

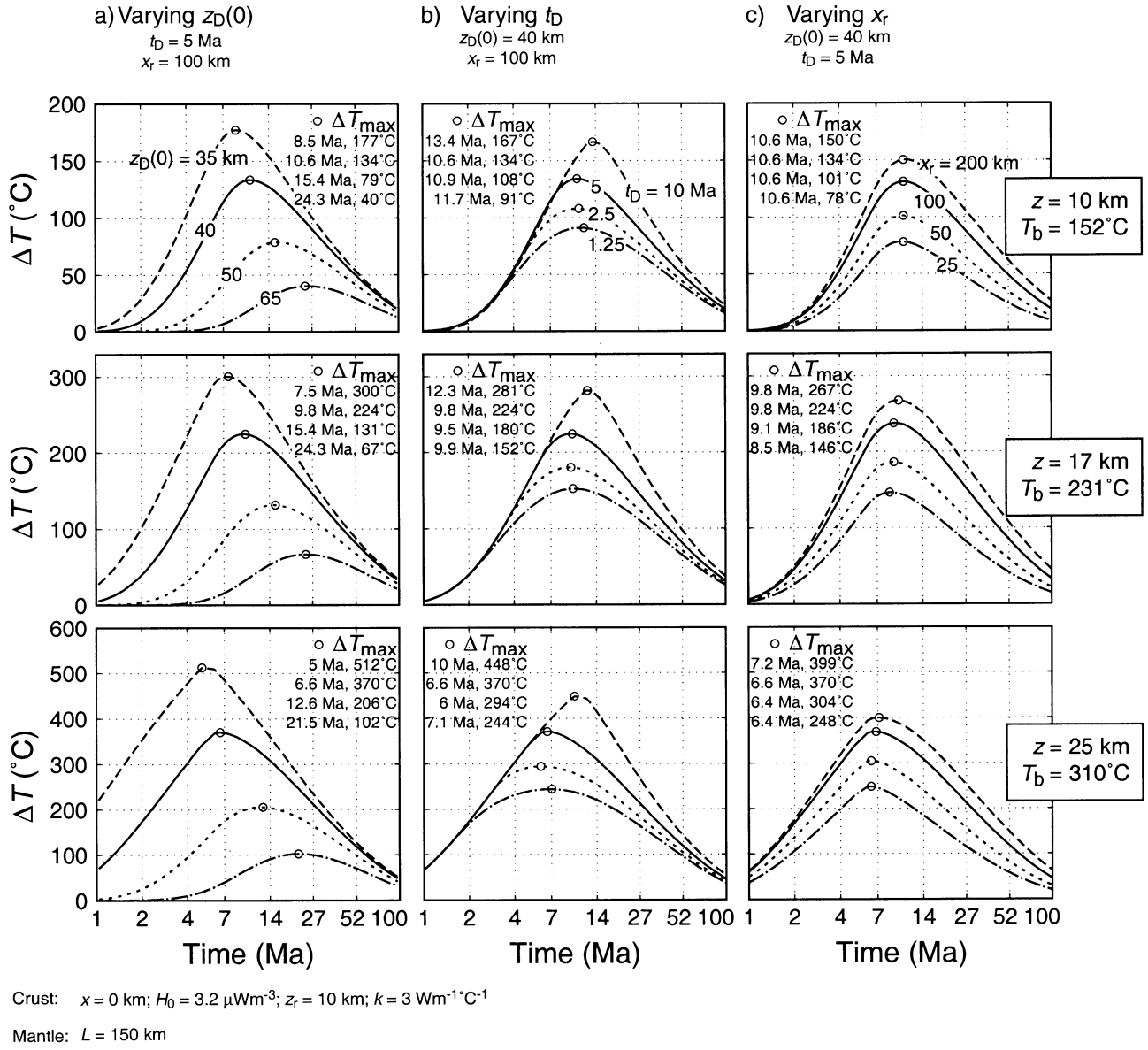

Fig. 7. ΔT–t diagrams at $x=0$ for $z=10$, 17 and 25 km, showing the influence of mantle anomaly parameters $z_D(0)$, t_D and x_r. The solid black curves in each row of panels represents the parameter combination $z_D(0)=40$ km, $t_D=5$ Ma and $x_r=100$ km, permitting direct comparison of the ΔT–t evolution and its sensitivity to variations in each parameter. (a) ΔT–t curves for $z_D(0)=35$, 40, 50 and 65 km, at constant t_D and x_r. (b) ΔT–t curves for $t_D=1.25$, 2.5, 5 and 10 Myr, at constant $z_D(0)$ and x_r. (c) ΔT–t curves for $x_r=25$, 50, 100 and 200 km, at constant $z_D(0)$ and t_D.

greater in the scenario where the ascent zone of the magma is thermally perturbed (Fig. 9b). Nevertheless, despite the size and high temperature of this intrusion, its thermal influence (via conductive cooling) on the host rocks is relatively fleeting. All points in the vicinity of the intrusion ($x=0$ or 33 km) attain ΔT_{max} within 3 Myr of emplacement, even at $z=10$ km, 7.5 km above the top surface of the pluton. Cooling is rapid, with ΔT being significantly diminished within 10 Myr of emplacement in all cases.

Despite the fact that 'regional' contact metamorphism of this nature takes place on a timescale demonstrably shorter than that of propagating thermal effects attributable to a mantle-related temperature anomaly, plutonism-related conductive heating has the capacity to elevate temperatures in the surrounding crust extremely rapidly. Consequently, the combination of mafic plutonism and a mantle temperature anomaly has the potential to generate a protracted thermal event in the middle crust commencing shortly after lithospheric removal. Mid-crustal temperatures may initially be raised by widespread plutonism, with the onset of heating attributable to the mantle temperature anomaly occurring before the intrusion-related

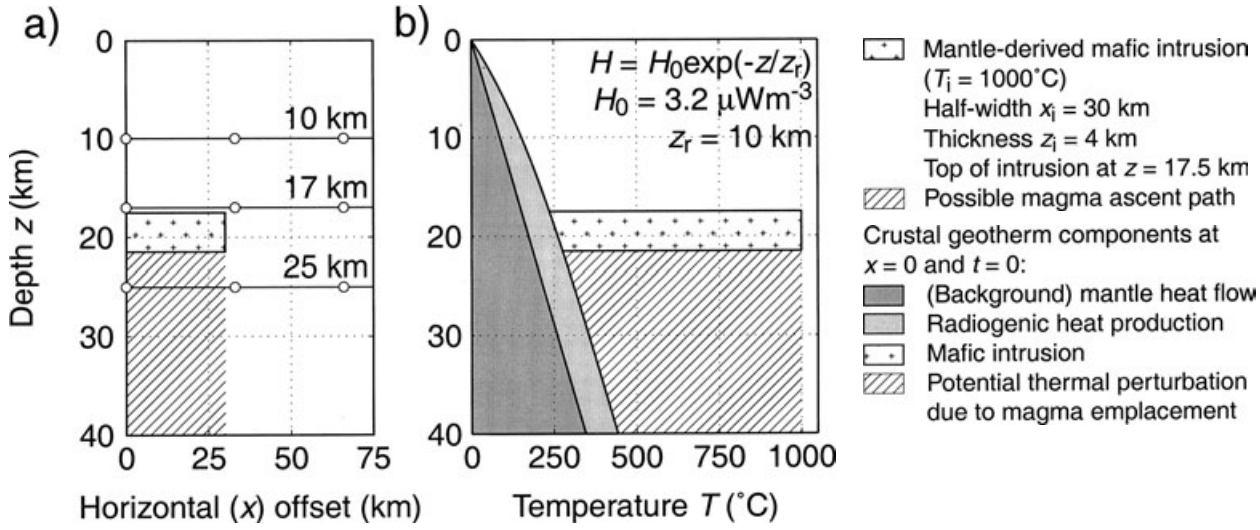

Fig. 8. (a) Diagram showing the location and size of the mafic pluton modelled. White circles represent points for which ΔT–t curves are calculated, and are identical to those in Fig. 4(a). The hatched area represents the crustal zone which may be thermally perturbed by the ascent of the magma. (b) Diagram showing the heat sources contributing to the crustal geotherm at $t=0$. The two thermal scenarios considered in detail in Fig. 9 correspond to the absence and presence (respectively) of the hatched region in this panel.

elevated temperature gradients have significantly dissipated.

Figure 10 shows ΔT–t curves for the points in Fig. 8(a), emphasising the relative crustal heating roles of mafic plutonism and the mantle temperature anomaly. Dashed lines represent the pluton in isolation, with and without elevated temperatures in the ascent zone of the magma (as in Fig. 9). The 'dot-dashed' line is the ΔT–t curve resulting from the mantle anomaly in the absence of intrusive activity (as in Fig. 5), and the thick solid lines indicate the ΔT–t curve resulting from the combined effects of mafic intrusion (for both modes of emplacement) initiated simultaneously with the mantle temperature anomaly. It is clear that there is significant overlap between the conductive cooling of the pluton and the onset of the thermal pulse originating from the basal temperature anomaly.

At $x=0$, which represents the lateral mid-point of the intrusion as well as the axis of the mantle temperature anomaly, ΔT values range up to 350 °C at $z=17$ km if temperatures are elevated in the magma ascent zone (see Fig. 9b), although these values are clearly sensitive to the assumed position of the intrusion. The associated delay in the conductive dissipation of this heat prolongs the interval over which ΔT remains above *c.* 300 °C, maintaining high temperatures in the middle crust until the thermal pulse due to the mantle anomaly begins to decay significantly (at $t\approx15$ Myr). Initial ($t\approx0$) values of ΔT at $z=17$ km are comparably high (peaking at $\Delta T=282$ °C) even when elevated temperatures are confined to the intrusive body (as in Fig. 9a). However, very rapid cooling sees ΔT decrease to approximately 130 °C within 2 Myr of emplacement, prior to the onset of thermal effects attributable to the mantle temperature anomaly, resulting in a double-peaked ΔT–t curve (solid grey lines in Fig. 10). Note that at $x=0$, the pluton-related ΔT peak is not fully visible because it occurs at $t<1$ Myr for all depths in Fig. 10. In addition, the increased distance between the points at $x=33$ km and the magmatic heat source greatly decreases the amplitude of the pluton-related ΔT peak relative to that of the ΔT peak attributable to mantle-related crustal heating. The transience of all pluton-related effects is well illustrated by the convergence of the ΔT–t curves following the attainment of the ΔT peak caused by the mantle anomaly, with ΔT remaining above 150 °C until $t\approx27$ Myr regardless of the mode of pluton emplacement.

Away from the axis of the anomaly and the mid-point of the intrusion, the intensity of the thermal pulse experienced by the crust is subdued and delayed, but the essential aspects of the interaction between the two heat sources remain unchanged. At $x=33$ km and $z=17$ km, initial ΔT values caused by the pluton are in the range 50–130 °C, depending strongly on the mode of emplacement (see Fig. 9). A consequence of the delay in the attainment of pluton-related peak ΔT is that overall crustal temperatures increase monotonically, as the rate of post-intrusion cooling is outstripped by the heating associated with the onset of the mantle-related thermal pulse. The mode of emplacement of the pluton makes little difference to the overall value of ΔT_{max} (195 °C if the ascent path of the magma is thermally perturbed, 166 °C if not) or the time at which it is attained, with $t\,(\Delta T_{max})=10$ and 13 Myr, respectively.

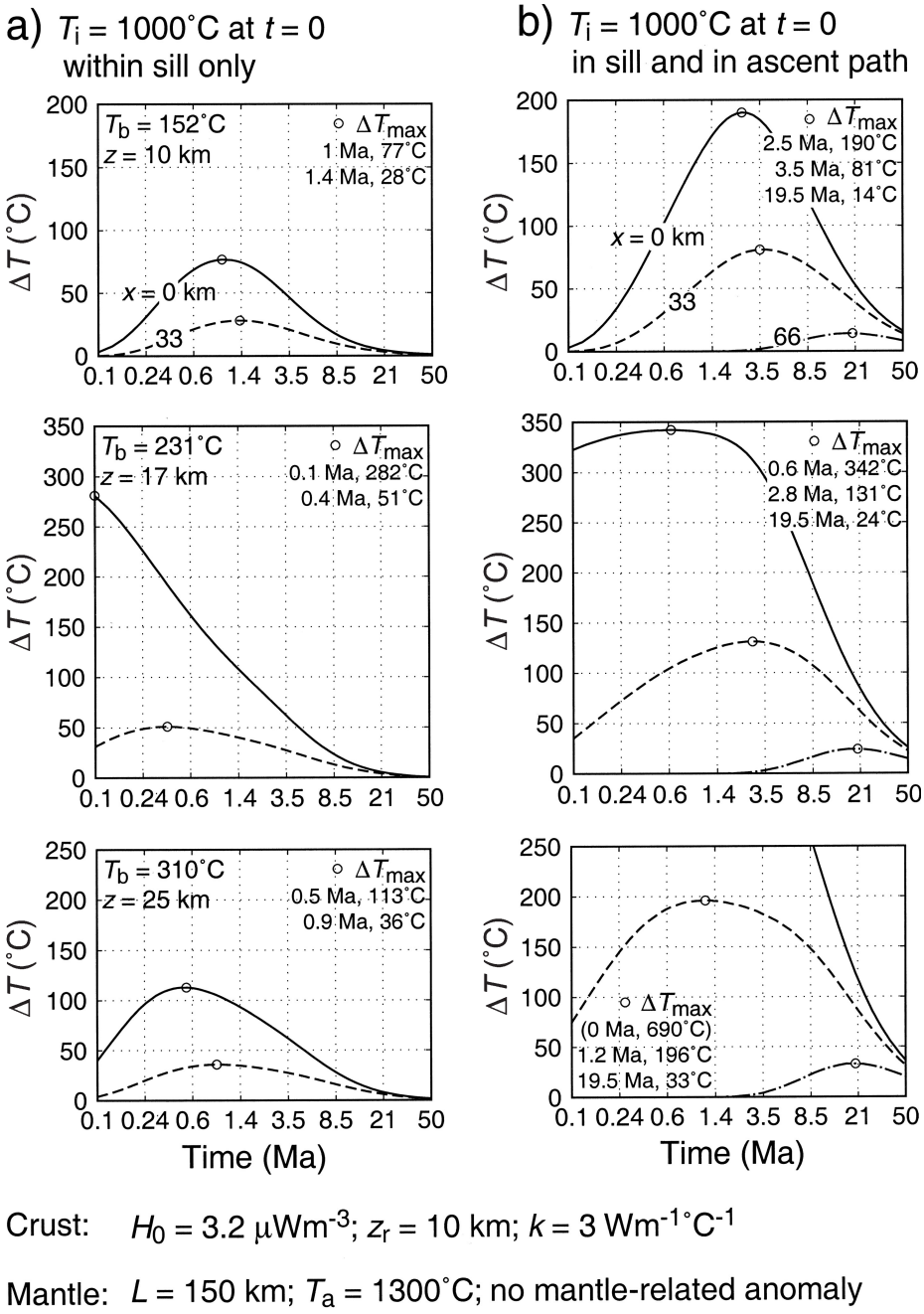

Fig. 9. ΔT–t curves resulting from emplacement of the intrusion shown in Fig. 8(a). (a) $T_i = 1000$ °C within the pluton only, with no thermal effect on the underlying crust. (b) $T_i = 1000$ °C within the pluton and its ascent path. Regardless of the mode of emplacement, all points in the vicinity of the pluton ($x = 0$ or 33 km) attain ΔT_{max} within 3 Myr of intrusion, and thermal effects have significantly dissipated within 10 Myr, with the exception of the point that lies within the ascent path ($x = 0$, $z = 25$ km).

Figure 10 shows that the combined influence of a mafic pluton and a mantle-related thermal pulse is capable of generating and maintaining elevated temperatures in the middle crust for an extended period, even when the duration of the mantle anomaly is relatively short. At a depth of 17 km, $\Delta T > 150$ °C at $x = 0$ for approximately 30 Myr following the initiation of thermal activity, when $t_D = 5$ Myr for the mantle pulse modelled. However, away from the immediate vicinity of the intrusion, the amplitude, timing and duration of the combined thermal pulse experienced by the crust does not differ significantly from that of the mantle anomaly operating in isolation, unless the pluton has heated its ascent path.

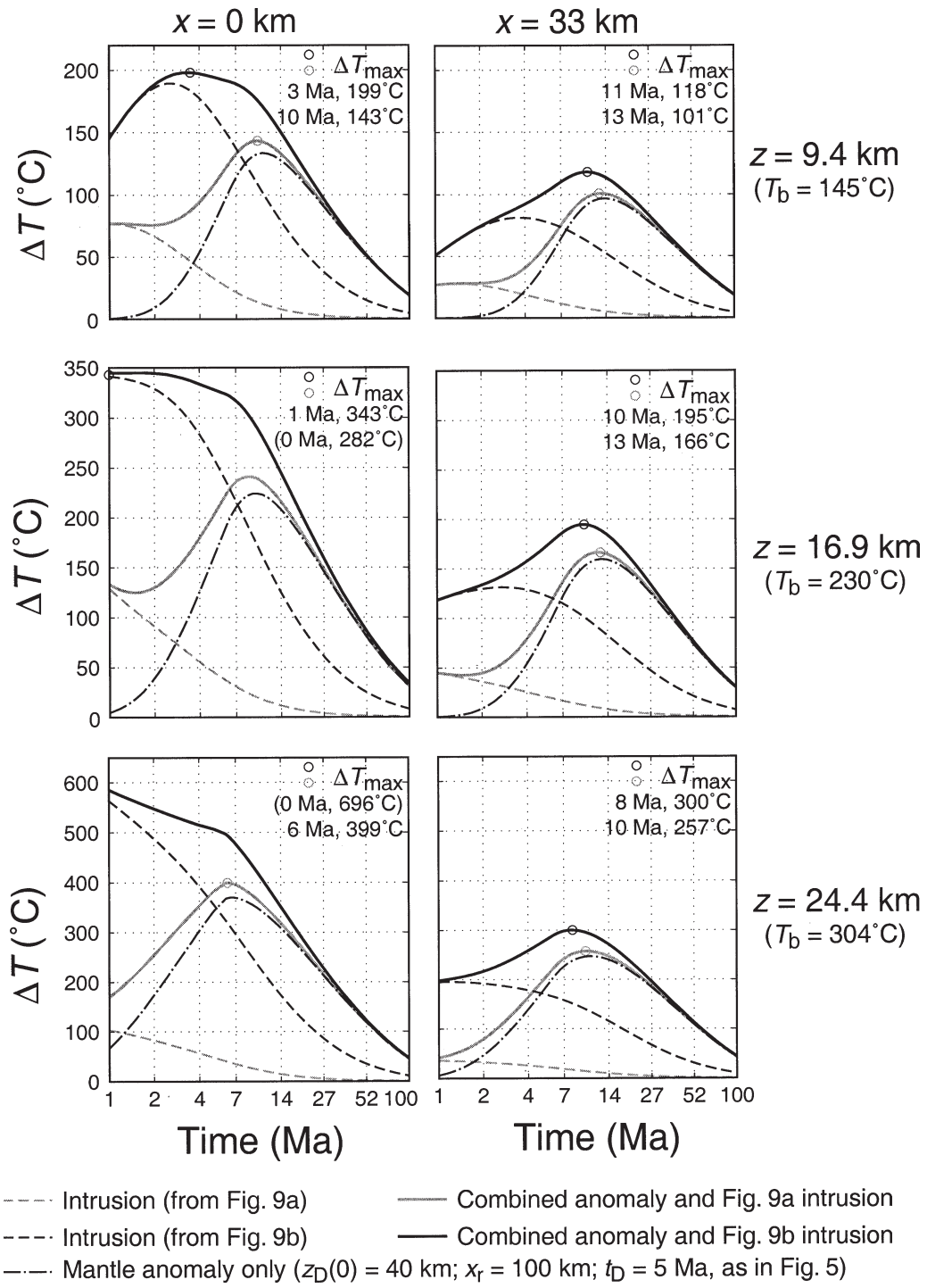

Fig. 10. ΔT–t paths at $x=0$ and 33 km for $z=10$, 17 and 25 km, highlighting the contributions of intrusion-related conductive heating and elevated mantle heat flow. At $x=0$, overall ΔT_{max} values are dictated by the initial T contrast between the intrusion and the host rocks when the intrusion thermally perturbs its ascent path. Mantle-related heating prolongs but does not intensify the thermal event. In contrast, if $T_i=1000$ °C within the body of the intrusion only, ΔT_{max} and $t(\Delta T_{max})$ coincide with the peak of the mantle-related heating event, except for points immediately adjacent to the intrusive body. At $x=33$ km, the thermal response of the crust to the two heat sources is delayed and diminished. ΔT_{max} and $t(\Delta T_{max})$ are insensitive to the mode of pluton emplacement, which instead primarily influences the pre-peak ΔT–t curve.

APPLICATION OF THE MODEL TO THE HALLS CREEK OROGEN

We now seek to evaluate the applicability of the numerical model developed above to the simulation of the thermal history preserved by rocks in the Central zone of the Halls Creek Orogen. The results are then used to establish constraints on the time at which the mantle-related thermal anomaly was initiated in the Halls Creek Orogen, based on the relative and absolute chronology of pre-1840 Ma plutonism and metamorphism in the Western and Central zones.

Comparison of the modelled *T–t* curves and the thermal history preserved by the central Halls Creek Orogen

One of the important predictions made by our numerical models concerns the way crustal cooling rates change with the size and duration of the mantle temperature anomaly, because it is often possible to place relatively tight constraints on the cooling rates of metamorphic rocks using modern thermochronological techniques. However, time-averaged cooling rate data from real metamorphic rocks are likely to reflect the sum of (i) decay of transient heat sources (such as the mantle-related thermal anomaly that forms the focus of this study), and (ii) exhumation-related cooling. Thus an important limitation of our model is the assumed uniform and time-invariant properties of the crust, precluding the direct comparison of the model results with observed *T–t* curves in 'real' orogenic belts. The models do not account for the particle paths experienced by such rocks, especially during exhumation. Therefore, in order to meaningfully compare the model and observed *T–t* curves, it is necessary to assess the relative contributions of tectonic denudation and decay of transient heat sources in the thermal record preserved by the rocks. If these components can be deconvolved, then the *P-T–t* data may be used to place constraints on the size and intensity of the transient heat sources responsible for metamorphism.

In the Tickalara Metamorphics, the available geological and thermochronological data suggest that $T_{max}=700$–750 °C and $P=400$–500 MPa (i.e. $z\simeq17$ km) at *c.* 1845 Ma, and $T\approx400$ °C at *c.* 1815 Ma (see Table 1 and references therein). Thus the total time-averaged cooling rate post-peak metamorphism $(\partial T/\partial t)_{mean}\approx-10\pm2$ °C Ma^{-1}, subject to the absence of direct temperature constraints in the post-1830 Ma part of the history. In addition, mid-crustal mafic magmatism may result in ΔT_{max} values up to 50–200 °C higher than those achieved at $z=17$ km during operation of the mantle temperature anomaly in isolation (Figs 8–10), depending on the proximity of the intrusion, the mode of pluton emplacement and the size of the mantle anomaly. In view of the presence of abundant and voluminous mafic intrusions within the Tickalara Metamorphics, we consider that T_{max} attributable specifically to a mantle-related heat source in the absence of plutonism is unlikely to exceed 550–600 °C at $z=17$ km.

Deconvolution of the relative contributions of tectonic denudation and decay of transient heat sources to the observed time-averaged cooling rate is complicated by the absence of suitable *P–T* data. However, rapid cooling immediately following the attainment of peak metamorphic conditions is precluded by the emplacement of the Mabel Downs Tonalite under amphibolite facies conditions, and within a D3 deformation regime dominated by the development of ductile structures, some 10–15 Myr after the granulite facies event at *c.* 1845 Ma (Fig. 2b, Table 1). In conjunction with the relatively shallow depth at which peak metamorphic temperatures were recorded, these data and relationships suggest that exhumation-related mid-crustal cooling was negligible in comparison with the decay of transient heat sources in the interval 1845–1830 Ma. However, the rate of crustal cooling associated with the decay of transient heat sources initiated pre-1845 Ma would have decreased significantly and rapidly post-1830 Ma, as the temperature contrast between the decaying mantle anomaly and the adjacent lithosphere progressively decreased. The development of regional-scale, post-1820 Ma brittle structures suggests that mid-crustal cooling resulting from exhumation became more important later in the history of the Halls Creek Orogen, and was instrumental in the maintenance of $(\partial T/\partial t)_{mean}\approx-10$ °C Ma^{-1} in the interval 1830–1810 Ma.

Figure 11(a) illustrates one possible combination of contributions from mantle anomaly decay and exhumation to the post-peak metamorphic *T–t* curve in Fig. 2(b), assuming that these two cooling mechanisms operate independently and that the measured *T–t* curve represents the time-integrated sum of their effects. For example, the vertical arrows at $t=1822$ Ma highlight that the overall temperature decrease assumed over the interval 1845–1822 Ma ($\Delta T\approx-230$ °C) is due to the combined effects of exhumation ($\Delta T\approx-90$ °C, mostly post-1830 Ma) and dissipation of the mantle temperature anomaly ($\Delta T\approx-140$ °C, most of which occurred in the interval 1845–1830 Ma). Figure 11(b) illustrates the evolution of the cooling rates associated with the *T–t* curves in Fig. 11(a), assuming uniform $(\partial T/\partial t)_{mean}\approx-10$ °C Ma^{-1} which constitutes the sum of the cooling rates associated with mantle anomaly decay and exhumation, respectively. For example, the vertical arrows at $t=1828$ Ma show that $(\partial T/\partial t)_{mean}\approx-10$ °C Ma^{-1} comprises $\partial T/\partial t\approx-3.2$ °C Ma^{-1} associated with the largely dissipated mantle temperature anomaly and $\partial T/\partial t\approx-6.8$ °C Ma^{-1} due to exhumation. The time-averaged contribution of each cooling rate over the time interval are approximately equal, i.e. $\approx-5\pm1$ °C Ma^{-1} in each case.

These estimates of the values of T_{max} and $(\partial T/\partial t)_{mean}$ may be used in conjunction with a fixed set of parameters defining the physical properties of our

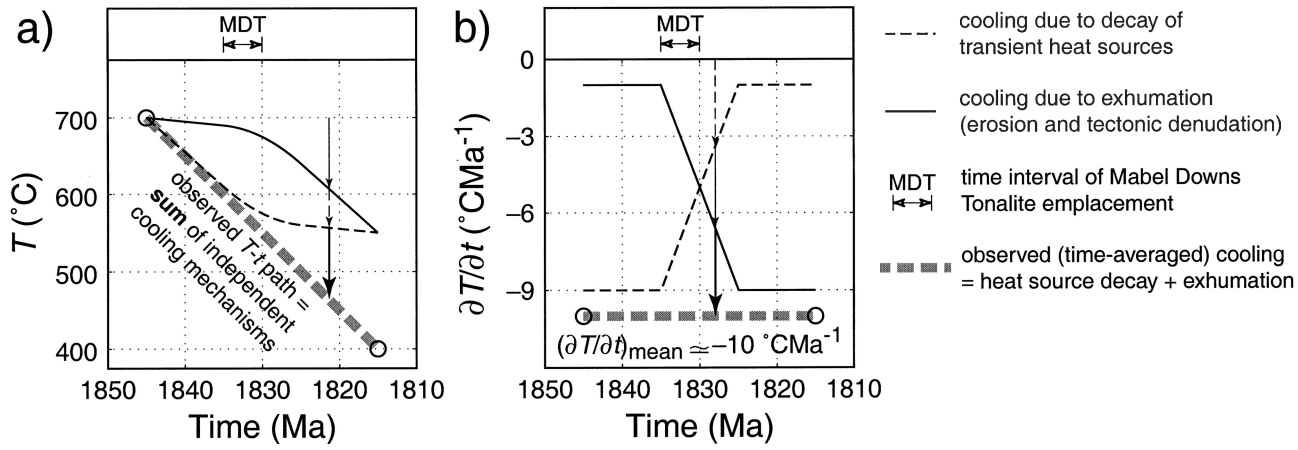

Fig. 11. (a) Temperature-time plot showing the possible relative contributions of (i) the decay of transient heat sources and (ii) exhumation (erosion and tectonic denudation) to the post-peak metamorphic segment of the *T–t* curve in Fig. 2(b), assuming that the time-equivalent effects of these two processes are cumulative. (b) Cooling rate-time plot for the *T–t* curves in (a), illustrating how the measured average cooling rate $(\partial T/\partial t)_{\text{mean}} \simeq -10$ °C Ma^{-1} is maintained over the interval 1845–1815 Ma. Note that the time-averaged contributions to $(\partial T/\partial t)_{\text{mean}}$ by transient heat source decay and exhumation are equal (each approximately -5 °C Ma^{-1}).

model lithosphere ($z_D = 40$ km, $k = 3$ Wm^{-1} °C^{-1}, $H_0 = 3.2$ μW m^{-3}, $z_r = 10$ km) to constrain the range of t_D and x_r values required for the mantle temperature anomaly. Figure 12 shows t_D–x_r space for each of the points shown in Fig. 8(a), contoured for $T_{\max}$ and $(\partial T/\partial t)_{\text{mean}}$. The lighter shade of grey represents the region in which $T_{\max} = 550 \pm 50$ °C and the darker shade is $(\partial T/\partial t)_{\text{mean}} = -5 \pm 1$ °C Ma^{-1}. The area of intersection of these two zones is largest at $z = 17$ km (compared to $z = 10$ km and $z = 25$ km), and at this intermediate depth the relevant range of $T_{\max}$ and $(\partial T/\partial t)_{\text{mean}}$ values may be generated (i) at $x = 0$ by a mantle anomaly of moderate size and intensity ($t_D \simeq 6$–11 Myr and $x_r = 75$ km), and (ii) at $x = 33$ km by a larger anomaly ($t_D \geq 12$ Myr and $x_r = 150$ km).

These data permit comparison of the timescales of the metamorphic processes predicted by the model with those observed in the Tickalara Metamorphics. The timescale of the model is correlated by defining $t = 0$ as the time at which mantle-derived mafic magmatism was initiated in the middle crust (as in Fig. 10), and we set $t = 0$ at *c.* 1860 Ma based on the U-Pb SHRIMP zircon ages of the oldest layered mafic-ultramafic intrusions in the Halls Creek Orogen (Table 1). We are interested in the time at which peak temperatures are attained $t(\Delta T_{\max})$ at $z = 17$ km for the range of mantle anomalies within the cross-hatched area in Fig. 12. At $x = 0$, $z = 17$ km, the range of $t(\Delta T_{\max})$ is 10.4 ± 0.2 Ma ($t_D = 7$ Myr, $x_r = 225$ km) to 14.8 ± 0.2 Ma ($t_D = 13$ Myr, $x_r = 75$ km). This range corresponds to the interval 1850–1845 Ma in the Halls Creek Orogen, which is in excellent agreement with published U–Pb monazite and zircon ages constraining peak metamorphism (Table 1, Oliver *et al.*, 1999; Bodorkos *et al.*, 2000b).

A generalised geological model for the evolution of the Halls Creek Orogen

The thermal history of the Halls Creek Orogen may be interpreted in the context of a mantle-related transient thermal anomaly initiated at *c.* 1860 Ma as the primary heat source for high-*T*, low-*P* metamorphism in the Central zone. Figure 13 is a cartoon showing the proposed evolution of generalised lithospheric columns representing the three major tectonostratigraphic zones of the Halls Creek Orogen over the interval of 1880–1810 Ma.

The earliest tectonic activity recognised in the western Halls Creek Orogen is related to accretion of the crust underlying the presently exposed Western zone to the eastern margin of the Kimberley Craton at *c.* 1880 Ma (Sheppard *et al.*, 1999; Griffin *et al.*, 2000), which was accompanied by thickening of the mantle lithosphere. Deposition of the Marboo Formation sediments in the Western zone and protoliths to the Tickalara Metamorphics in the Central zone over the interval 1870–1860 Ma was accompanied by collapse and 'breakoff' of the subducting slab at *c.* 1860 Ma, broadly synchronous with voluminous 1865–1850 Ma granite plutonism and associated metamorphism in the Western zone (Sheppard *et al.*, 1995; Tyler *et al.*, 1999) are attributed to this event (Fig. 13a, b, see also fig. 14 of Griffin *et al.*, 2000).

It is likely that sedimentation in the Western and Central zones was curtailed by uplift as the isostatic response to asthenospheric upwelling and the initiation of the mantle-related temperature anomaly. Emplacement of the oldest layered mafic-ultramafic intrusions in the Western and Central zones commenced at *c.* 1860 Ma (Fig. 13b, see also Hoatson, 1997), and modelling of magnetic and gravity data

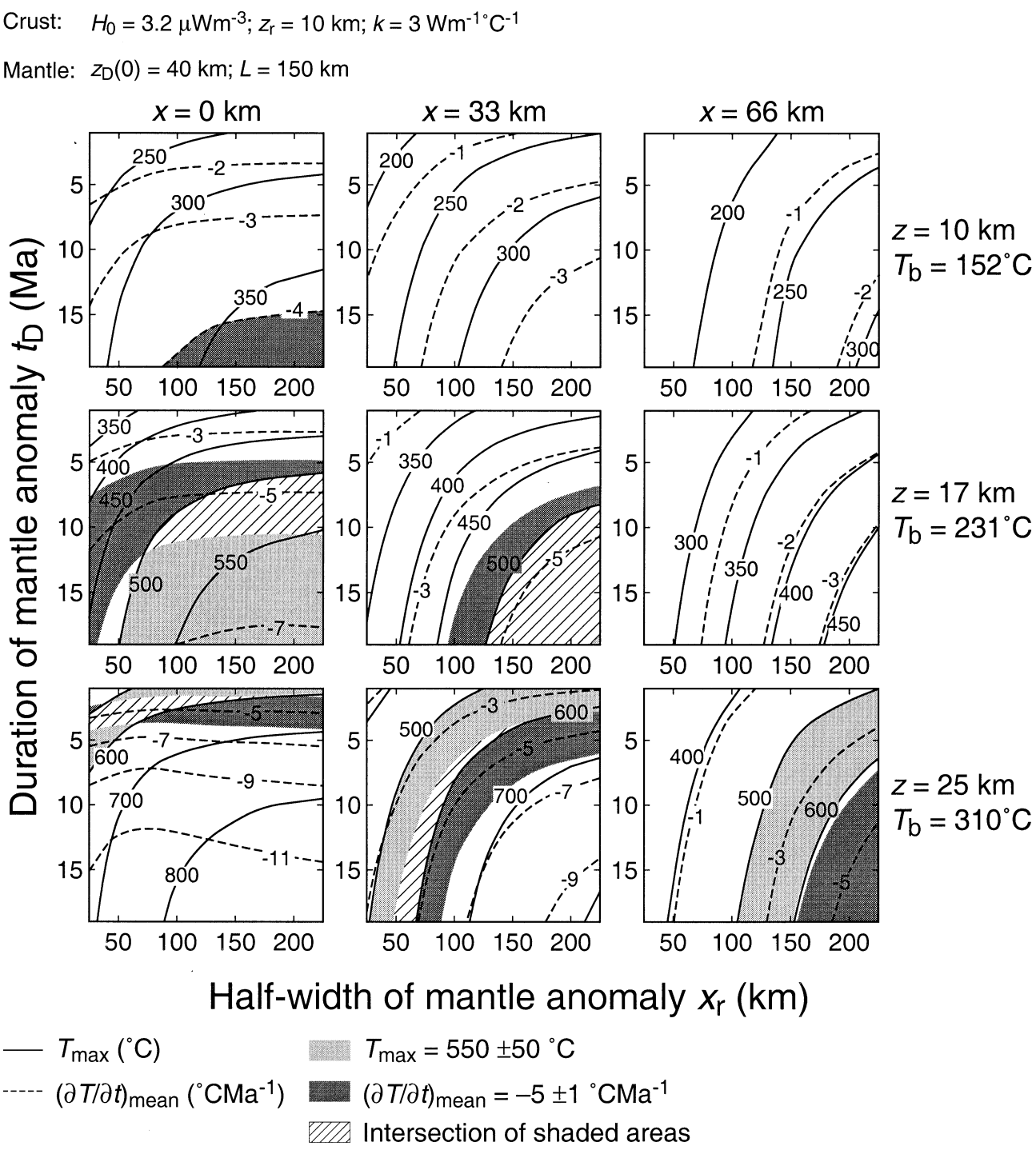

Fig. 12. Plots of x_r–t_D space contoured for T_{max} and $(\partial T/\partial t)_{mean}$ for the points shown in Fig. 8(a). The light grey indicates the region where T_{max} = 500–600 °C, the dark grey represents $(\partial T/\partial t)_{mean} = -5 \pm 1$ °C Ma^{-1} and the cross-hatched area shows the intersection of these two regions, which is maximised at depth z = 17 km. At the axis of the anomaly (x = 0 km), T_{max} and $(\partial T/\partial t)_{mean}$ are largely independent of x_r when x_r > 100 km. Away from the axis of the anomaly (x = 33 km), T_{max} and $(\partial T/\partial t)_{mean}$ are largely independent of t_D when t_D > 5 Myr.

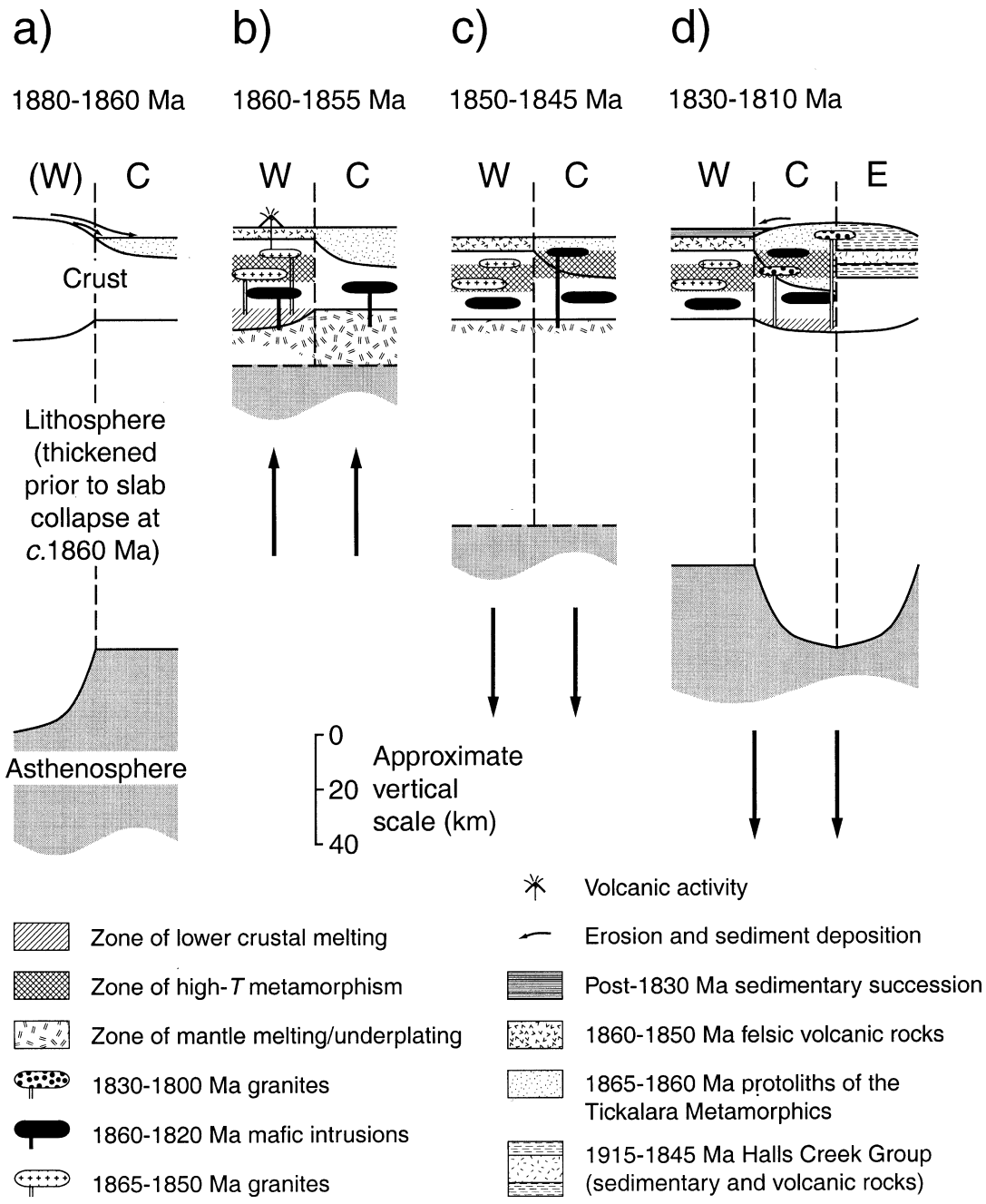

Fig. 13. Generalised lithospheric sections portraying the evolution of the three major tectono-stratigraphic zones in the Halls Creek Orogen in the interval 1880–1810 Ma. Approximate 'time-pin' locations are marked on the *T*–*t* path in Fig. 2(b). W, C and E = Western, Central and Eastern zones, respectively. Dashed vertical lines demark schematic boundaries between lithospheric columns, and do not represent juxtaposing faults. (a) Accretion of an exotic terrane along the eastern margin of the Kimberley Craton at *c.* 1880 Ma resulted in moderate thickening of the crust, and the generation of 'post-collisional' granitic magmas beneath the Western zone (cf. Griffin *et al.*, 2000). The Marboo Formation and protoliths to the Tickalara Metamorphics were deposited in marginal basins. (b) Collapse and/or 'breakoff' of the subducting slab at *c.* 1860 Ma was accompanied by granitic plutonism (and associated metamorphism) in the Western zone. Upwelling of hot asthenospheric material over several million years probably resulted in extensive underplating of the crust beneath the Western and Central zones, coincident with the onset of layered mafic-ultramafic plutonism in the middle crust. (c) Mafic magmatism diminished post-1850 Ma as the mantle lithosphere cooled and thickened. Peak metamorphism in the Central zone at *c.* 1845 Ma and a prolonged cooling history resulted from the conductive propagation of the mantle-derived heat pulse applied to the base of the crust 15–20 Myr earlier. (d) Collision of the Kimberley and North Australian cratons generated post-1830 Ma granites (Sheppard *et al.*, 1999), and erosion of the elevated collisional zone provided detritus for the 1835–1750 Ma sedimentary overlap succession, the oldest units of which were deposited atop rocks of the Western zone.

(Gunn & Meixner, 1998) suggests that underplating mafic magmas at depth comprise a volume sufficient to significantly raise mid-crustal temperatures in the short term, in addition to inducing partial melting and the generation of felsic magmas in the lower crust (e.g. Ellis, 1987; Huppert & Sparks, 1988; Warren & Ellis, 1996).

Peak metamorphism throughout the Central zone at *c.* 1845 Ma probably reflected the conductively propagated thermal effect of the elevated mantle heat flow into the middle crust, and was accompanied by smaller volumes of mafic intrusions as the mantle lithosphere cooled and thickened (Fig. 13c). Collision of the Kimberley Craton (comprising the amalgamated Western and Central zones) and the North Australian Craton (Eastern zone) commenced at *c.* 1835 Ma, and the oldest granites intruding the Central zone post-date peak metamorphism by only 10–15 Myr (Fig. 13d). Younger granites 'stitch' all three zones by *c.* 1810 Ma (Sheppard *et al.*, 1997).

CONCLUSIONS

Surface heat flow data place important constraints on the chemical composition of the crust (McLennan & Taylor, 1996), and thus provide insights into the potential role of radiogenic heat production as a heat source for regional metamorphism. The presence of significant concentrations of radionuclides in the lower crust will be reflected in elevated surface heat flow values in comparison to 'average' continental crust, especially in low-*P* metamorphic belts where the thickness of high heat-producing surficial material removed by erosion and/or tectonic denudation is presumably limited by preserved peak metamorphic pressures. It is likely that high-*T*, low-*P* metamorphic belts such as the Halls Creek Orogen, which are characterised by surface heat flow lower than that of average continental crust, require an alternative heat source.

This study has shown that the conductive propagation of a transient heat pulse through the base of the crust (resulting from a large-scale thermal anomaly in the upper mantle lithosphere) has the potential to generate regionally extensive high-*T*, low-*P* metamorphic rocks. Temperatures in the middle and upper portions of the crust may be raised significantly and rapidly, with ΔT_{max} values ranging from 50–500 °C, depending primarily on the thermal properties of the crust (k, H_0 and z_r), the depth at which the temperature anomaly is initiated in the upper mantle (z_D) and the duration over which it is dynamically maintained (t_D). The timescale over which crustal heating occurs is directly related to z_D, i.e. the vertical distance between the mid-crustal section of interest and the zone where $T \approx T_a$ over the interval $0 > t > t_D$. When $z_D = 40$ km, ΔT_{max} values are attained approximately 10–15 Myr after initiation of the anomaly (Fig. 7b), and the delay before attainment of ΔT_{max} increases with larger z_D (20–25 Myr when $z_D = 65$ km, see Fig. 7a).

Our results also illustrate the potential importance of the interaction between advective and conductive transfer of anomalous mantle-derived heat in the thermal record of plutonism and metamorphism preserved by the crust. In general, advective heat transfer (via the ascent of mantle-derived magmas and their emplacement in the middle crust) will be rapid, and the thermal effects of 'regional contact' metamorphism accompanying such plutonism are likely to be short-lived. In contrast, the rate of conductive propagation and dissipation of the thermal 'front' attributable to a large-scale, deep-seated heat source is relatively slow. Consequently, if the advection of mantle-derived magmas is broadly synchronous with the initiation of the thermal anomaly at depth in the mantle, temporal overlap between decaying pluton-related heating and the progressively intensifying of the conductively propagating thermal front has the potential to generate a prolonged thermal event in the middle crust. This scenario is especially applicable to the central Halls Creek Orogen, which is characterised by a number of 1860–1855 Ma layered mafic-ultramafic intrusions that predate the thermal peak of regional metamorphism by 10–15 Myr and are not spatially associated with the highest-grade metamorphic rocks. The temporal relationships are consistent with pluton emplacement accompanying initiation of the mantle-related thermal anomaly at $t = 0$, followed by the regional attainment of peak metamorphic conditions at $t \approx 15$ Myr (i.e. *c.* 1845 Ma).

When coupled with mantle-derived mafic plutonism and intrusive activity related to lower crustal anatexis, anomalous basal heat flux has the potential to be a major cause of high-*T*, low-*P* metamorphism (Ellis, 1987; Sandiford, 1989). Orogenic belts with a combination of geological and thermal characteristics best explained by a large-scale transient heat source are widely separated in space and time, ranging from the Cretaceous Ryoke fold belt in Japan (e.g. Brown, 1998 and references therein) to the Late Archaean Slave Province of northern Canada (e.g. Kusky, 1990; King *et al.*, 1992), providing a compelling argument for mantle-related crustal heating in at least some tectonic settings.

ACKNOWLEDGEMENTS

This work was carried out while S.B. was in receipt of a Curtin University Postgraduate Scholarship, and the project was funded by an Australian Research Council Large Grant awarded to N.H.S.O. We thank S. Sheppard and I. Tyler of the Geological Survey of Western Australia for informative and constructive discussions. The suggestions of J. Huntoon and an

anonymous reviewer resulted in significant improvements to the manuscript. This is Tectonics Special Research Centre Publication No. 154.

REFERENCES

Barton, M. D. & Hanson, R. B., 1989. Magmatism and the development of low-pressure metamorphic belts: implications from the western United States and thermal modeling. *Geological Society of America Bulletin*, **101,** 1051–1065.

Batt, G. E. & Braun, J., 1997. On the thermomechanical evolution of compressional orogens. *Geophysical Journal International*, **128,** 364–382.

Bird, P., 1979. Continental delamination and the Colorado Plateau. *Journal of Geophysical Research*, **84,** 7561–7571.

Bodorkos, S., Cawood, P. A. & Oliver, N. H. S., 2000a. Timing and duration of syn-magmatic deformation in the Mabel Downs Tonalite, northern Australia. *Journal of Structural Geology*, **22,** 1181–1198.

Bodorkos, S., Cawood, P. A., Oliver, N. H. S. & Nemchin, A. A., 2000b. Rapidity of orogenesis in the Paleoproterozoic Halls Creek Orogen, northern Australia: evidence from SHRIMP zircon data, CL zircon images and mixture modeling studies. *American Journal of Science*, **300,** 60–82.

Bodorkos, S., Oliver, N. H. S. & Cawood, P. A., 1999. Thermal evolution of the central Halls Creek Orogen, northern Australia. *Australian Journal of Earth Sciences*, **46,** 453–465.

Brown, M., 1998. Ridge–trench interactions and high-T–low-P metamorphism, with particular reference to the Cretaceous evolution of the Japanese Islands. In: *What Drives Metamorphism and Metamorphic Reactions? Special Publication 138.* (eds Treloar, P. J. & O'Brien, P. J.), pp. 137–169. Geological Society, London.

Cull, J. P., 1982. An appraisal of Australian heat-flow data. *BMR Journal of Australian Geology and Geophysics*, **7,** 11–21.

Davies, J. H. & von Blanckenburg, F., 1995. Slab breakoff: a model of lithosphere detachment and its test in the magmatism and deformation of collisional orogens. *Earth and Planetary Science Letters*, **129,** 85–102.

De Yoreo, J. J., Lux, D. R. & Guidotti, C. V., 1991. Thermal modelling in low-pressure/high-temperature metamorphic belts. *Tectonophysics*, **188,** 209–238.

De Yoreo, J. J., Lux, D. R., Guidotti, C., Decker, E. & Osberg, P., 1989. The Acadian thermal history of western Maine. *Journal of Metamorphic Geology*, **7,** 169–190.

Ellis, D. J., 1987. Origin and evolution of granulites in normal and thickened crust. *Geology*, **15,** 167–170.

Etheridge, M. A., Rutland, R. W. R. & Wyborn, L. A. I., 1987. Orogenesis and tectonic process in the Early to Middle Proterozoic of northern Australia. In: *Proterozoic Lithospheric Evolution Geodynamics Series, 17*, (ed. Kroner, A.) pp. 131–147. American Geophysical Union, Washington DC.

Fowler, C. M. R., 1990. *The Solid Earth: an Introduction to Global Geophysics*. Cambridge University Press, Cambridge.

Griffin, T. J., Page, R. W., Sheppard, S. & Tyler, I. M., 2000. Tectonic implications of Palaeoproterozoic post-collisional, high-K felsic igneous rocks from the Kimberley region of northwestern Australia. *Precambrian Research*, **101,** 1–23.

Gunn, P. J. & Meixner, A., 1998. The nature of the basement to the Kimberley Block, northwestern Australia. *Geological Society of Australia Abstracts*, **49,** 191.

Hanson, R. B. & Barton, M. D., 1989. Thermal development of low-pressure metamorphic belts: results from two-dimensional numerical models. *Journal of Geophysical Research*, **94,** 10363–10377.

Hoatson, D. M., 1993. Correlation of structurally disrupted layered ultramafic-mafic intrusions in the East Kimberley: is Big Ben part of the Panton intrusion? *AGSO Research Newsletter*, **19,** 9.

Hoatson, D., 1997. Geology and mineralisation of the Palaeoproterozoic layered mafic-ultramafic intrusions of the Halls Creek Orogen, Western Australia. In: *Palaeoproterozoic Tectonics and Metallogenesis: Comparative Analysis of Parts of the Australian and Fennoscandian Shields* (eds Rutland, R. W. R. & Drummond, B. J.). *AGSO Record 1997/44*, pp. 61–64. Australian Geological Survey Organisation, Canberra.

Hoatson, D. M. & Tyler, I. M., 1993. Prospective layered mafic-ultramafic intrusions in the East Kimberley. *AGSO Research Newsletter*, **18,** 8–9.

Houseman, G. A., McKenzie, D. P. & Molnar, P., 1981. Convective instability of a thickened boundary layer and its relevance for the thermal evolution of continental convergent belts. *Journal of Geophysical Research*, **86,** 6115–6132.

Houseman, G. A. & Molnar, P., 1997. Gravitational (Rayleigh-Taylor) instability of a layer with non-linear viscosity and convective thinning of continental lithosphere. *Geophysical Journal International*, **128,** 125–150.

Huerta, A. D., Royden, L. H. & Hodges, K. V., 1996. The interdependence of deformational and thermal processes in mountain belts. *Science*, **273,** 637–639.

Huerta, A. D., Royden, L. H. & Hodges, K. V., 1998. The thermal structure of collisional orogens as a response to accretion, erosion, and radiogenic heating. *Journal of Geophysical Research*, **103,** 15287–15302.

Huppert, H. E. & Sparks, R. S. J., 1988. The generation of granitic magmas by intrusion of basalt into continental crust. *Journal of Petrology*, **29,** 599–624.

Jaeger, J. C., 1959. Temperatures outside a cooling intrusive sheet. *American Journal of Science*, **257,** 44–54.

Jaeger, J. C., 1964. Thermal effects of intrusions. *Reviews of Geophysics*, **2,** 443–466.

Jamieson, R. A., Beaumont, C., Fullsack, P. & Lee, B., 1998. Barrovian regional metamorphism: where's the heat? In: *What Drives Metamorphism and Metamorphic Reactions? Special Publication 138* (eds Treloar, P. J. & O'Brien, P. J.), pp. 23–51. Geological Society, London.

King, J. E., Davis, W. J. & Relf, C., 1992. Late Archean tectono-magmatic evolution of the central Slave Province, Northwest Territories. *Canadian Journal of Earth Sciences*, **29,** 2156–2170.

Kusky, T. M., 1990. Evidence for Archean ocean opening and closing in the southern Slave Province. *Tectonics*, **9,** 1533–1563.

Loosveld, R. J. H. & Etheridge, M. A., 1990. A model for low-pressure facies metamorphism during crustal thickening. *Journal of Metamorphic Geology*, **8,** 257–267.

Lubimova, E. A. & Nikitina, V. N., 1975. On heat flow singularities over mid-ocean ridges. *Journal of Geophysical Research*, **80,** 232–243.

Lux, D. R., De Yoreo, J. J., Guidotti, C. V. & Decker, E. R., 1986. Role of plutonism in low-pressure metamorphic belt formation. *Nature*, **323,** 794–797.

Mathur, S. P. & Shaw, R. D., 1982. Australian orogenic belts: evidence for evolving plate tectonics? *Earth Evolution Sciences*, **4,** 281–308.

McKenzie, D., 1967. Some remarks on heat flow and gravity anomalies. *Journal of Geophysical Research*, **72,** 6261–6273.

McLaren, S., Sandiford, M. & Hand, M., 1999. High radiogenic heat-producing granites and metamorphism – An example from the western Mount Isa inlier, Australia. *Geology*, **27,** 679–682.

McLennan, S. M. & Taylor, S. R., 1996. Heat flow and the chemical composition of continental crust. *Journal of Geology*, **104,** 369–377.

Miyashiro, A., 1973. *Metamorphism and Metamorphic Belts*. George Allen & Unwin, London.

Morton, J. L. & Sleep, N. H., 1985. A mid-ocean ridge thermal model: constraints on the volume of axial hydrothermal heat flux. *Journal of Geophysical Research*, **90,** 11345–11353.

Myers, J. S., Shaw, R. D. & Tyler, I. M., 1996. Tectonic evolution of Proterozoic Australia. *Tectonics*, **15,** 1431–1446.

Nyblade, A. A. & Pollack, H. N., 1993. A global analysis of heat flow from Precambrian terrains: implications for the thermal structure of Archean and Proterozoic lithosphere. *Journal of Geophysical Research*, **98,** 12207–12218.

Oliver, N. H. S. & Barr, T. D., 1997. The geometry and evolution of magma pathways through migmatites of the Halls Creek Orogen, Western Australia. *Mineralogical Magazine*, **61,** 3–14.

Oliver, N. H. S., Bodorkos, S., Nemchin, A. A., Kinny, P. D. & Watt, G. R., 1999. Relationships between zircon U-Pb SHRIMP ages and leucosome type in migmatites of the Halls Creek Orogen, Western Australia. *Journal of Petrology*, **40,** 1553–1575.

Page, R. W., Hoatson, D. M., Sun, S. & Foudoulis, C., 1995a. High-precision geochronology of Palaeoproterozoic layered mafic-ultramafic intrusions in the East Kimberley. *AGSO Research Newsletter*, **22,** 7–8.

Page, R. W., Tyler, I. M. & Blake, D. H., 1995b. Geochronology of magmatism and high-grade metamorphism, Kimberley region, W.A. *Australian Conference on Geochronology and Isotope Geoscience (ACOG 3) Abstracts*, pp. 25, Curtin University, Perth.

Ruppel, C. & Hodges, K. V., 1994. Pressure-temperature-time paths from two-dimensional thermal models: prograde, retrograde and inverted metamorphism. *Tectonics*, **13,** 17–44.

Sacks, P. E. & Secor, D. T., 1990. Delamination in collisional orogens. *Geology*, **18,** 999–1002.

Sandiford, M., 1989. Horizontal structures in granulite terrains: a record of mountain building or mountain collapse? *Geology*, **17,** 449–452.

Sandiford, M. & Hand, M., 1998. Australian Proterozoic high-temperature, low-pressure metamorphism in the conductive limit. In: *What Drives Metamorphism and Metamorphic Reactions? Special Publication 138*, (eds Treloar, P. J. & O'Brien, P. J.), pp. 109–120. Geological Society, London.

Sandiford, M., Martin, N., Zhou, S. & Fraser, G., 1991. Mechanical consequences of granite emplacement during high-T, low-P metamorphism and the origin of 'anticlockwise' PT paths. *Earth and Planetary Science Letters*, **107,** 164–172.

Sandiford, M. & Powell, R., 1986. Deep crustal metamorphism during continental extension: modern and ancient examples. *Earth and Planetary Science Letters*, **79,** 151–158.

Sandiford, M. & Powell, R., 1991. Some remarks on high-temperature, low-pressure metamorphism in convergent orogens. *Journal of Metamorphic Geology*, **9,** 333–340.

Sclater, J. G., Anderson, R. N. & Bell, M. L., 1971. Elevation of ridges and evolution of the central eastern Pacific. *Journal of Geophysical Research*, **76,** 7888–7915.

Sclater, J. G., Jaupart, C. & Galson, D., 1980. The heat flow through oceanic and continental crust and the heat loss of the Earth. *Reviews of Geophysics and Space Physics*, **18,** 269–311.

Sheppard, S., Griffin, T. J. & Tyler, I. M., 1995. Geochemistry of felsic igneous rocks from the southern Halls Creek Orogen. *GSWA Record 1995/4.* Geological Survey of Western Australia, Perth.

Sheppard, S., Griffin, T. J. & Tyler, I. M., 1997. The tectonic setting of granites in the Halls Creek and King Leopold Orogens, northwest Australia. In: *Palaeoproterozoic Tectonics and Metallogenesis: Comparative Analysis of Parts of the Australian and Fennoscandian Shields* (eds Rutland, R. W. R. & Drummond, B. J.), pp. 107–109. *AGSO Record 1997/44*, Australian Geological Survey Organisation, Canberra.

Sheppard, S., Tyler, I. M., Griffin, T. J. & Taylor, W. R., 1999. Palaeoproterozoic subduction-related and passive margin basalts in the Halls Creek Orogen, northwest Australia. *Australian Journal of Earth Sciences*, **46,** 679–690.

Sleep, N. H., 1969. Sensitivity of heat flow and gravity to the mechanism of sea-floor spreading. *Journal of Geophysical Research*, **74,** 542–549.

Sleep, N. H., 1975. Formation of oceanic crust: Some thermal constraints. *Journal of Geophysical Research*, **80,** 4037–4042.

Sleep, N. H., 1996. Lateral flow of hot plume material ponded at sub-lithospheric depths. *Journal of Geophysical Research*, **101,** 28065–28083.

Sonder, L. J. & Chamberlain, C. P., 1992. Tectonic controls of metamorphic field gradients. *Earth and Planetary Science Letters*, **111,** 517–535.

Sproule, R. A., Lambert, D. D. & Hoatson, D. M., 1999. Re-Os isotopic constraints on the genesis of the Sally Malay Ni-Cu-Co deposit, East Kimberley, Western Australia. *Lithos*, **47,** 89–106.

Thompson, P. H., 1989. Moderate overthickening of thinned sialic crust and the origin of granitic magmatism and regional metamorphism in low-P–high-T terranes. *Geology*, **17,** 520–523.

Thornett, J. R., 1986. Evolution of a high-grade metamorphic terrain in the Proterozoic Halls Creek Mobile Zone, Western Australia. *PhD Thesis, University of Western Australia, Perth*.

Trudu, A. & Hoatson, D. M., 1996. Depths of emplacement of Precambrian layered intrusions in the East Kimberley. *AGSO Research Newsletter*, **25,** 10–12.

Turcotte, D. L. & Schubert, G., 1982. *Geodynamics: The Application of Continuum Physics to Geological Problems*. John Wiley & Sons, New York.

Tyler, I. M., Griffin, T. J., Page, R. W. & Shaw, R. D., 1995. Are there terranes within the Lamboo Complex of the Halls Creek Orogen? *Geological Survey of Western Australia Annual Review*, 1993/94, 37–46.

Tyler, I. M., Page, R. W. & Griffin, T. M., 1999. Depositional age and provenance of the Marboo Formation from SHRIMP U-Pb zircon geochronology: Implications for the early Palaeoproterozoic tectonic evolution of the Kimberley region, Western Australia. *Precambrian Research*, **95,** 225–243.

Warren, R. G. & Ellis, D. J., 1996. Mantle underplating, granite tectonics and metamorphic P-T-t paths. *Geology*, **24,** 663–666.

Wells, P. R. A., 1980. Thermal models for the magmatic accretion and subsequent metamorphism of continental crust. *Earth and Planetary Science Letters*, **46,** 253–265.

Wickham, S. M. & Oxburgh, E. R., 1987. Low-pressure regional metamorphism in the Pyrenees and its implications for the thermal evolution of rifted continental crust. *Philosophical Transactions of the Royal Society of London*, **321A,** 219–242.

Zielhuis, A. & van der Hilst, R. D., 1996. Upper-mantle shear velocity beneath eastern Australia from inversion of waveforms from SKIPPY portable arrays. *Geophysical Journal International*, **127,** 1–16.

Received 17 August 2000; revision accepted 23 April 2001.